HEALTH AND MEDICINE

Copyright © 2018 The Authors, some rights reserved; exclusive licensee American Association for the Advancement of Science. No claim to original U.S. Government Works. Distributed under a Creative Commons Attribution NonCommercial License 4.0 (CC BY-NC).

Synthetic matrix enhances transplanted satellite cell engraftment in dystrophic and aged skeletal muscle with comorbid trauma

Woojin M. Han[1,2], Shannon E. Anderson[2,3], Mahir Mohiuddin[2,3], Daniela Barros[1,2,4,5,6], Shadi A. Nakhai[2,7], Eunjung Shin[2,7], Isabel Freitas Amaral[4,5,8], Ana Paula Pêgo[4,5,6,8], Andrés J. García[1,2]*, Young C. Jang[2,3,7]*

Muscle satellite cells (MuSCs) play a central role in muscle regeneration, but their quantity and function decline with comorbidity of trauma, aging, and muscle diseases. Although transplantation of MuSCs in traumatically injured muscle in the comorbid context of aging or pathology is a strategy to boost muscle regeneration, an effective cell delivery strategy in these contexts has not been developed. We engineered a synthetic hydrogel-based matrix with optimal mechanical, cell-adhesive, and protease-degradable properties that promotes MuSC survival, proliferation, and differentiation. Furthermore, we establish a biomaterial-mediated cell delivery strategy for treating muscle trauma, where intramuscular injections may not be applicable. Delivery of MuSCs in the engineered matrix significantly improved in vivo cell survival, proliferation, and engraftment in nonirradiated and immunocompetent muscles of aged and dystrophic mice compared to collagen gels and cell-only controls. This platform may be suitable for treating craniofacial and limb muscle trauma, as well as postoperative wounds of elderly and dystrophic patients.

INTRODUCTION

Skeletal muscle generates force to enable movement and support vital functions such as deglutition and respiration. Although healthy muscle exhibits remarkable adaptive and regenerative capacities, its function declines with comorbidity of severe physical trauma, aging, and disease (*1*–*5*). Inadequate regeneration of muscle begets debilitating consequences, including long-term disabilities and reduced quality of life (*5*–*7*). Current clinical interventions for muscle trauma entail muscle flap transfer and surgical suture, but these treatments alone do not completely regenerate the damaged muscle (*3*, *8*–*10*). Clinical strategies that effectively regenerate traumatically injured muscle in comorbidity with aging and muscle pathology currently do not exist and are in great critical need.

Muscle satellite cells (MuSCs) are muscle-resident stem cells that play an indispensable role in myogenesis, and their function centrally dictates the regenerative capacity of muscle in the context of injury, aging, and disease (*11*–*15*). Upon injury, quiescent MuSCs ($Pax7^+$/$MyoD^-$) activate to give rise to proliferating myoblasts ($Pax7^+$/$MyoD^+$) that undergo myogenic differentiation or fusion with existing myofibers (*1*, *2*). Asymmetric division of MuSCs maintains muscle homeostasis, where this process is critical for regeneration of damaged myofibers and repopulation of the stem cell reservoir through self-renewal for ensuing regenerative needs (*16*–*18*). However, the intrinsic function and quantity of MuSCs decline with aging (*13*, *19*–*23*) and neuromuscular diseases, such as Duchenne muscular dystrophy (DMD) (*14*, *15*), and contribute to the diminished regenerative potential of muscle. For example, one mechanism that causes age-associated decline in MuSC function and number is that MuSCs lose the ability to asymmetrically divide from abnormal Janus kinase–signal transducer and activator of transcription and p38 signaling and undergo cellular senescence from elevated $p16^{INK4A}$ (*19*, *21*, *22*). In DMD, dystrophin-deficient MuSCs exhibit impaired mitosis and loss of asymmetric division (*14*). Dysregulation of MuSC function ultimately results in depletion of the MuSC reservoir and defective muscle regenerative potential. The regenerative potential further diminishes upon traumatic muscle injuries, such as bone-muscle polytrauma, laceration, crush, and severe burn, where MuSCs undergo concurrent activation and cell death (*24*–*27*). Although approaches aimed to replenish functional MuSCs in traumatically injured muscles in the comorbid context of aging or chronic pathology may be an effective strategy to boost degenerating muscle function, successful and translatable approaches to transplant MuSCs in traumatically injured aged or pathologic muscles have not yet been developed.

Transplantation of MuSCs into injured, aging, and dystrophic muscles results in engraftment and repopulation of the quiescent MuSC pool (*28*–*31*). This strategy has significant potential for administering MuSCs as a cellular source for stem cell therapy for muscle injury, sarcopenia, and muscular dystrophy. However, previous proof-of-principle transplantation experiments have been conducted on skeletal muscles that were cardiotoxin/notexin/$BaCl_2$-injured, irradiated, and/or immunodeficient, limiting their clinical translatability (*28*–*31*). Furthermore, direct delivery of cells via injection has challenges at the translational level, including massive donor cell death and cellular dispersion, severely limiting its therapeutic potential (*32*, *33*). Only 1 to 20% of the transplanted cells survive in the host tissue due to the harsh inflammatory environment, and the surviving donor cells exhibit limited function (*32*, *33*). Note that cell delivery via injection may not always be applicable in traumatic injuries, where the structural integrity of the muscle is often severely compromised to receive an injection. To address these limitations, naturally derived biomaterials, such as decellularized matrix, collagen, hyaluronic acid, fibrin, and alginate

[1]Woodruff School of Mechanical Engineering, Georgia Institute of Technology, Atlanta, GA 30332, USA. [2]Parker H. Petit Institute for Bioengineering and Bioscience, Georgia Institute of Technology, Atlanta, GA 30332, USA. [3]Coulter Department of Biomedical Engineering, Georgia Institute of Technology, Atlanta, GA 30332, USA. [4]Instituto de Engenharia Biomédica, Universidade do Porto, Porto, Portugal. [5]Instituto de Investigação e Inovação em Saúde, Universidade do Porto, Porto, Portugal. [6]Instituto de Ciências Biomédicas Abel Salazar, Universidade do Porto, Porto, Portugal. [7]School of Biological Sciences, Georgia Institute of Technology, Atlanta, GA 30332, USA. [8]Faculdade de Engenharia, Universidade do Porto, Porto, Portugal.
*Corresponding author. Email: andres.garcia@me.gatech.edu (A.J.G.); young.jang@gatech.edu (Y.C.J.)

Downloaded from http://advances.sciencemag.org/ on July 5, 2019

hydrogels, have been used to facilitate the delivery of myogenic cells to the muscle (*34*–*45*). However, naturally derived materials are susceptible to lot-to-lot variability, potential pathogen transfer, and difficulty in controlling the material's microstructure, mechanical properties, and degradability; these limitations hinder their translatability, wide applicability, and systematic investigation of material-MuSC interactions to improve engraftment efficacy (*46*). Furthermore, previous studies used nonquiescent myoblasts that had been expanded in vitro, and thus, knowledge on how the biochemical and biophysical properties of these materials affect quiescent MuSC activities is limited. Synthetic matrices, on the other hand, offer a promising alternative to natural biomaterials, as biochemical and biophysical properties can be modularly altered to investigate three-dimensional (3D) cellular functions in a systematic manner. To that end, we hypothesized that a synthetic biofunctional hydrogel, which presents promyogenic cell adhesive peptides and defined mechanical, transport, and on-demand degradation properties, could be engineered to support MuSC activities and serve as a delivery vehicle to enhance the engraftment of donor cells in traumatically injured, nonirradiated, and immunocompetent skeletal muscle in the context of aging and muscular dystrophy.

Here, we report an engineered, synthetic hydrogel-based matrix that promotes primary MuSC survival, proliferation, and differentiation in 3D. MuSCs exhibited robust survival, proliferation, and differentiation in synthetic hydrogels functionalized with the integrin-targeting Arg-Gly-Asp (RGD) adhesive peptide and cross-linked with protease-degradable peptides. Proliferation of MuSCs was further enhanced through optimization of the hydrogel's mechanical properties and mesh size. Transplantation of MuSCs using this engineered synthetic matrix to the supramuscular locus of cryo-injured tibialis anterior (TA) muscles of dystrophic (*mdx-4CV*) and aged (23 months old) mice significantly improved donor cell engraftment compared to cell-free and collagen gel controls. Collectively, the results establish this engineered synthetic matrix as a versatile platform for stem cell therapy in the context of skeletal muscle injury, aging, and neuromuscular diseases.

RESULTS

Modular hydrogel platform as a synthetic MuSC matrix

To engineer a biofunctional matrix for MuSC culture and delivery, we selected a synthetic hydrogel platform based on a four-arm poly(ethylene glycol) (PEG) macromer, with its ends functionalized with maleimide groups (PEG-4MAL) as the base material. The PEG-4MAL platform exhibits excellent biocompatibility in vivo and cytocompatibility with various cell types, including pancreatic islets and skeletal myoblasts (*47*–*50*). Furthermore, PEG-4MAL hydrogels have significant advantages over naturally derived extracellular matrices and other synthetic gels, such as the ability to independently tune mechanical, structural, and biochemical properties and minimization of lot-to-lot variability (*50*, *51*). In this synthetic platform, the maleimide groups in PEG-4MAL macromers are efficiently reacted with thiol-containing cell-adhesive peptides through Michael-type addition, enabling stoichiometric functionalization of the macromer. The remaining maleimide groups are then reacted with cysteine-flanked peptides (for example, GCRDVPMSMRGGDRCG) to cross-link macromers to yield a hydrogel with a highly defined structural network (Fig. 1A). The cytocompatible maleimide-thiol reaction can be performed in the presence of cells to yield cell-laden 3D constructs. Thus, we sought to engineer a biofunctional matrix capable of promoting MuSC survival, proliferation, and differentiation using the PEG-4MAL hydrogel platform by evaluating the effects of adhesive ligand type, mechanical and diffusive transport properties, and protease degradability (Fig. 1A).

RGD-presenting synthetic matrix supports myogenesis

An important consideration for engineering a synthetic matrix for adherent cells is the presentation of context-dependent, cell-adhesive ligands, as cell adhesion is a necessary process for survival, proliferation, migration, and differentiation (*52*–*54*). To identify optimal cell-adhesive ligands for MuSC function, we evaluated the effects of cell-binding synthetic peptides found in fibronectin and laminin, prominent extracellular matrix proteins constituting the native MuSC niche (table S1). We isolated $Pax7^+$ primary MuSCs by flow cytometry using a previously established set of markers ($CD45^-$, $CD11b^-$, $Ter119^-$, $Sca1^-$, $CXCR4^+$, and $\beta1$ $integrin^+$; Fig. 1B) (*28*) and encapsulated the cells as nonaggregated single cells in 4% (w/v) PEG-4MAL hydrogels (20-kDa macromer) containing either 1.0 mM RGD, RDG (scrambled control), YIGSR, or C16 synthetic peptides and cross-linked with protease-degradable peptides (fig. S1). All these hydrogel formulations exhibit equivalent mechanical, diffusive transport, and protease-degradable properties (*51*). After 6 days of culture in growth media containing basic fibroblast growth factor (FGF-2), MuSCs cultured in RGD-presenting hydrogels proliferated and formed noncircular $MyoD^+$ myogenic colonies, compared to RDG-presenting ($P < 0.0001$), YIGSR-presenting ($P < 0.05$), and C16-presenting ($P < 0.001$) hydrogels (Fig. 1, C and D). For RGD-presenting hydrogels, cell packing density within a myogenic colony was significantly lower compared to the other hydrogel formulations ($P < 0.0001$), suggesting cellular migration (Fig. 1, C and E). Furthermore, myogenic colonies formed in RGD-presenting hydrogels were significantly larger compared to colonies formed in RDG-, YIGSR-, and C16-presenting hydrogels ($P < 0.0001$; Fig. 1, C and F). However, when cell proliferation was assessed via EdU (5-ethynyl-2′-deoxyuridine) incorporation, we observed no statistical differences among hydrogels containing different cell-adhesive peptides on both days 3 and 6 of culture (Fig. 1, C and G, and fig. S2A). Furthermore, MuSCs in RGD-, RDG-, C16-, and YIGSR-presenting hydrogels exhibited similar levels of MuSC activation (>60% $Pax7^+$ and >95% $MyoD^+$ activated MuSCs per colony; fig. S2, B and C) after 72 hours of culture, indicating that potential differences in activation state did not contribute to the differential myogenic colony formation. Notably, MuSCs cultured in RGD-presenting hydrogels exhibited significantly less $TUNEL^+$ cells compared to MuSCs in scrambled RDG-presenting hydrogels at day 1 after encapsulation ($P < 0.05$), indicating that hydrogels presenting the RGD cell-adhesive peptide promote cell survival and subsequently support the formation of robust myogenic colonies compared to hydrogels presenting scrambled RDG control peptide (Fig. 1, H and I).

Cellular fusion is a major hallmark of differentiated myocytes. To determine whether RGD-presenting hydrogels support MuSC differentiation, we mixed GFP^+ and $TdTomato^+$ MuSCs in a 1:1 ratio and encapsulated them within RGD- or RDG-presenting hydrogels. We reasoned that fused GFP^+ and $TdTomato^+$ cells would exhibit both fluorescent proteins in the cytosol, indicative of differentiation and fusion (fig. S3A). To prime differentiation, we initially cultured MuSCs in either RGD- or RDG-presenting hydrogels in growth media with daily supplementation of FGF-2 for 6 days and then in differentiation media for an additional 4 days. Cells cultured in RDG-presenting hydrogels did not fuse, and cells remained in multicellular clusters homogeneously, composed of either GFP^+ or $TdTomato^+$ myoblasts (Fig. 1J and fig. S3B). In contrast, cells cultured in RGD-presenting hydrogels were morphologically distinct, where the cells were elongated and spread (Fig. 1J and

Downloaded from http://advances.sciencemag.org/ on July 5, 2019

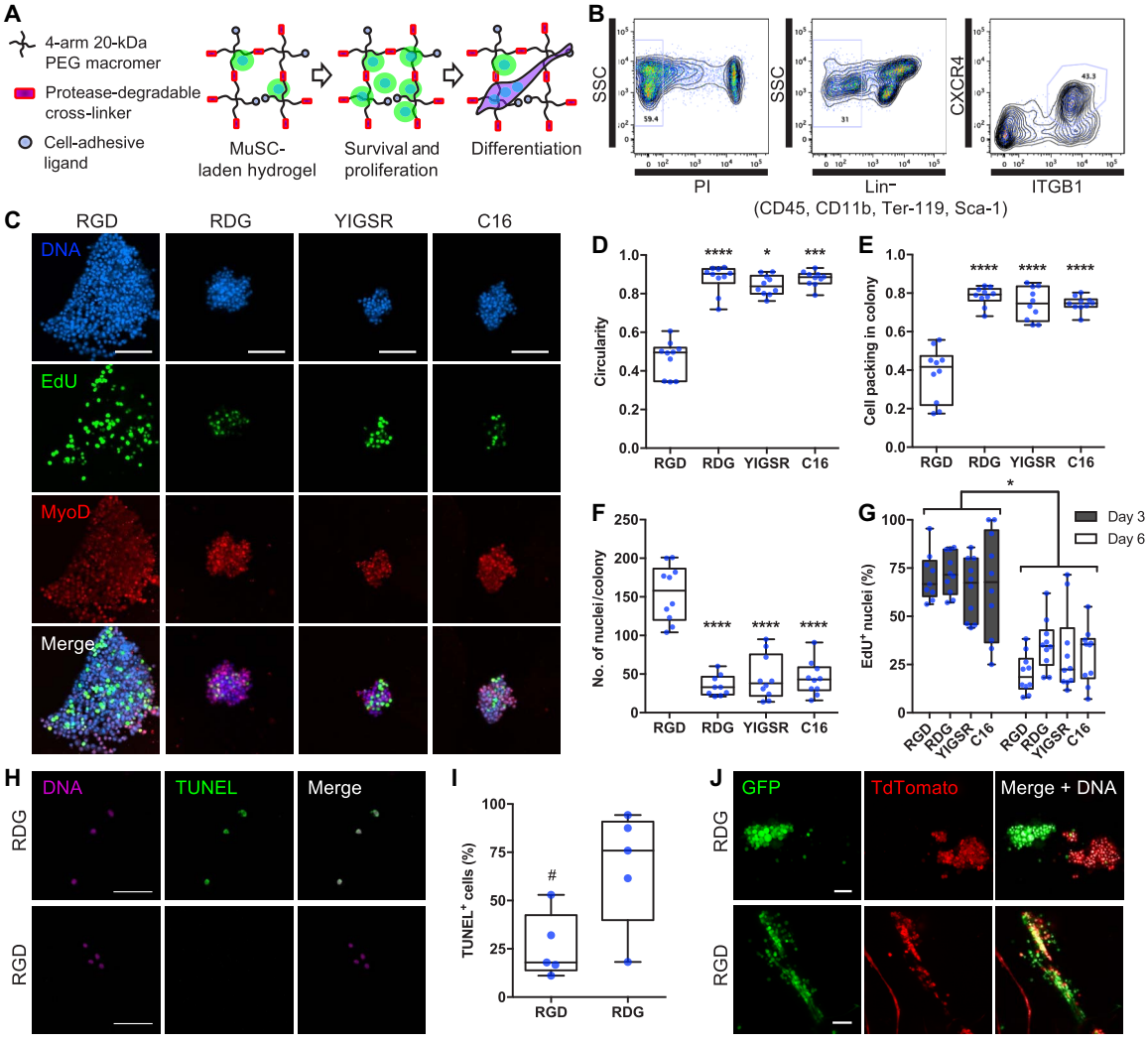

Fig. 1. RGD-presenting PEG-4MAL hydrogels promote MuSC survival, proliferation, and differentiation. (**A**) Schematic of cell-laden hydrogel. Synthetic hydrogel platform can be biofunctionalized with cell-adhesive ligands and protease-degradable cross-linkers. (**B**) Representative fluorescence-activated cell sorting plot of MuSCs. SSC, side scatter; PI, propidium iodide; ITGB1, β1 integrin. (**C**) Representative *z*-projections of myogenic colonies formed in PEG-4MAL hydrogels presenting synthetic cell adhesive peptides (day 6). Scale bars, 100 μm. (**D**) Quantification of myogenic colony circularity. $n = 9$ and 10 colonies. $^{*}P < 0.05$, $^{***}P < 0.001$, and $^{****}P < 0.0001$ versus RGD via Kruskal-Wallis with Dunn's test. (**E**) Quantification of myogenic colony cell packing density. $n = 9$ and 10 colonies. $^{****}P < 0.0001$ versus all groups via one-way analysis of variance (ANOVA) with Tukey's test. (**F**) Quantification of myogenic colony size. $n = 9$ and 10 colonies. $^{****}P < 0.0001$ versus all groups via one-way ANOVA with Tukey's test. (**G**) Quantification of myogenic colony proliferation. $n = 9$ and 10 colonies. $^{*}P < 0.05$ via two-way ANOVA with Sidak's test. (**H**) Representative *z*-projections of DNA and terminal deoxynucleotidyl transferase–mediated deoxyuridine triphosphate nick end labeling (TUNEL) staining (day 1). Scale bars, 50 μm. (**I**) Quantification of TUNEL^{+} cells. $n = 5$ hydrogels. $^{\#}P < 0.05$ via unpaired two-tailed *t* test. (**J**) Representative *z*-projections of green fluorescent protein–positive (GFP^{+}) and TdTomato^{+} MuSCs. Cells were cultured in growth media for 6 days and then in differentiation media for 4 days. GFP/TdTomato-fused cells appear yellow. Scale bars, 100 μm.

fig. S3B). Moreover, cell fusion events were present, indicated by multinucleated myotubes expressing both GFP^{+} and TdTomato^{+} in the cytosol, with a significantly higher fusion index compared to control RDG-presenting hydrogels ($P < 0.0001$; Fig. 1J and fig. S3, B and C). Differentiated myotubes exhibited spontaneous contraction in the RGD-presenting hydrogels, indicating functional differentiation of MuSC (movie S1). Despite the marked differences in cellular fusion and morphology, cells in both RGD- and RDG-presenting hydrogels stained positive for desmin and myosin heavy chain upon culturing in differentiation media (fig. S3D) and exhibited similar levels of myogenin and desmin gene expression (fig. S3E). This result suggests that the reduced serum content of the differentiation media primes the cells to differentiate, but cells are unable to undergo fusion in the non-adhesive RDG-presenting hydrogels, corroborating the importance of cell-adhesive ligands in the cellular fusion process. β3 integrin, a major target of RGD tripeptide sequence, has been shown to be an essential factor for myotube formation (*54*). Collectively, these results indicate that presentation of RGD adhesive peptide in PEG-4MAL hydrogels promotes MuSC in vitro survival, proliferation, and differentiation.

PEG-4MAL macromer density modulates MuSC proliferation

The biophysical properties of the extracellular matrix have a profound impact on cellular functions (*55*). In the PEG-4MAL hydrogel system, altering the PEG-4MAL polymer density can modulate the mechanical

Downloaded from http://advances.sciencemag.org/ on July 5, 2019

properties and mesh size. As the polymer density increases (from 3 to 6%, w/v), we introduce more cross-links to the system, resulting in the formation of a tighter polymer network and increased hydrogel storage modulus (from 150 to 300 Pa; Fig. 2, A and B). As tighter polymer networks are formed with increasing polymer density, the mesh size decreases (Fig. 2, A and C). To evaluate the effects of polymer density on MuSC function, we encapsulated and cultured freshly isolated MuSCs within 3 to 6% 20-kDa PEG-4MAL hydrogels containing 1.0 mM RGD and cross-linked with protease-degradable peptides. MuSCs cultured in 3 and 4% PEG-4MAL hydrogels formed significantly larger myogenic colonies compared to cells in 6% PEG-4MAL hydrogels at day 4 ($P < 0.01$ and $P < 0.001$, respectively; Fig. 2, D and E). Furthermore, the number of colonies formed in 3% PEG-4MAL hydrogels was significantly greater compared to that in 5 and 6% PEG-4MAL hydrogels ($P < 0.05$; Fig. 2, D and F). Finally, 3 and 4% PEG-4MAL hydrogels promoted significantly increased cell proliferation compared to 6% PEG-4MAL hydrogels ($P < 0.05$ and $P < 0.01$, respectively; Fig. 2, G and H), collectively indicating that 3 to 4% PEG-4MAL hydrogels support optimal MuSC proliferation and myogenic colony formation.

To determine the effects PEG-4MAL polymer density on MuSC activation, we examined $Pax7^+/MyoD^+$ expression of MuSCs in 4 and 6% PEG-4MAL hydrogels presenting 1.0 mM RGD and cross-linked with protease-degradable peptides at 76 hours after encapsulation. Although no differences in MyoD expression were observed, myogenic

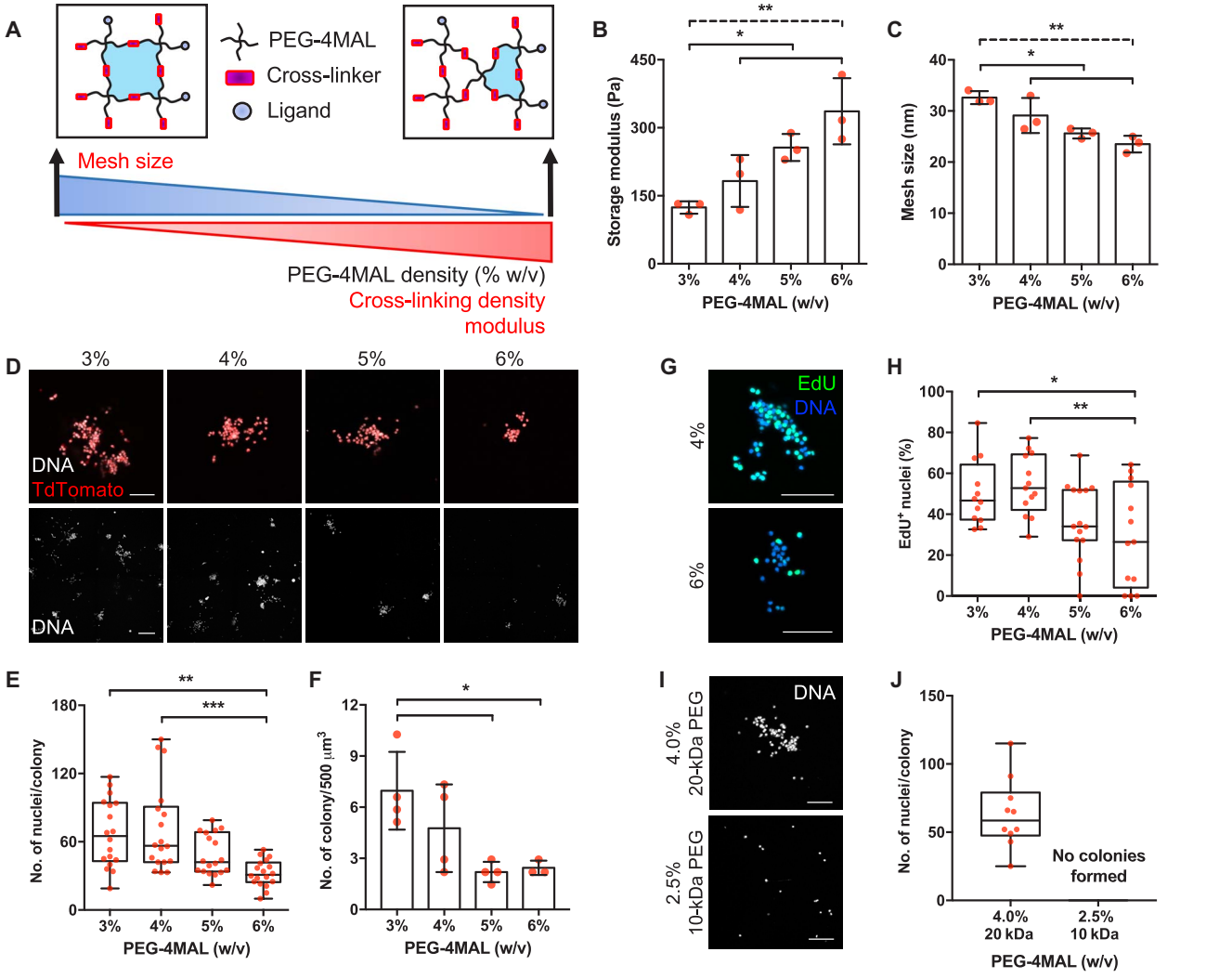

Fig. 2. PEG-4MAL macromer density modulates MuSC proliferation. (**A**) Schematic describing the changes in hydrogel mesh size and mechanical properties as a function of PEG-4MAL macromer density. (**B**) Storage modulus of hydrogels for different macromer densities. $n = 3$ hydrogels. $^*P < 0.05$ (solid line) and $^{**}P < 0.01$ (dashed line) via one-way ANOVA with Tukey's test. (**C**) Estimation of hydrogel mesh size based on the measured storage modulus. $n = 3$ hydrogels. $^*P < 0.05$ (solid line) and $^{**}P < 0.01$ (dashed line) via one-way ANOVA with Tukey's test. (**D**) Representative *z*-projections of myogenic colonies formed in PEG-4MAL hydrogels as a function of macromer density (day 4). Scale bars, 100 μm (top row) and 250 μm (bottom row). Percentage values indicate PEG-4MAL macromer density. (**E** and **F**) Quantification of myogenic colony ($n = 18$ colonies) and density ($n = 3$ and 4 hydrogels). $^*P < 0.05$, $^{**}P < 0.01$, and $^{***}P < 0.001$ via one-way ANOVA with Tukey's test. (**G**) Representative *z*-stack projections of EdU-labeled myogenic colonies (day 4). Scale bars, 100 μm. (**H**) Quantification of EdU^+ nuclei. $n = 12$ to 15 colonies. $^*P < 0.05$ and $^{**}P < 0.01$ via one-way ANOVA with Tukey's test. (**I**) Representative *z*-projections of MuSCs cultured in 4% 20-kDa and 2.5% 10-kDa PEG-4MAL hydrogels (day 4). Scale bars, 100 μm. (**J**) Quantification of myogenic colonies. $n = 10$ colonies. Bar graphs are presented as mean ± SD.

Downloaded from http://advances.sciencemag.org/ on July 5, 2019

colonies formed in 6% PEG-4MAL hydrogels exhibited significantly decreased levels of Pax7 expression compared to those formed in 4% PEG-4MAL hydrogels (fig. S4, A and B).

To assess whether the increased cell proliferation with decreasing macromer density is an effect of mesh size or mechanical properties, we encapsulated and cultured MuSCs in 2.5% 10-kDa PEG-4MAL and 4% 20-kDa PEG-4MAL hydrogels, both presenting 1.0 mM RGD and cross-linked with protease-degradable peptides. The 2.5% 10-kDa PEG-4MAL hydrogels have decreased solute diffusivity compared to 4% 20-kDa PEG-4MAL hydrogels ($P < 0.05$) due to the reduced molecular weight of the macromer while exhibiting comparable mechanical properties ($P > 0.05$) due to similar average cross-link density (fig. S5, A to F). MuSCs cultured in 2.5% 10-kDa PEG-4MAL did not form myogenic colonies on day 4, whereas colonies readily formed in 4% 20-kDa PEG-4MAL hydrogels (Fig. 2, I and J), suggesting that mesh size imparts a significant impact on the proliferation capacity of MuSCs in a 3D-culture setting.

Matrix degradability is required for MuSC function

Extracellular matrix degradability is an important factor for dynamic remodeling of the cellular microenvironment (*56*). We hypothesized that the degradability of the synthetic PEG-4MAL hydrogel is a critical feature for MuSC function, including survival and proliferation. To test this hypothesis, we encapsulated freshly isolated TdTomato$^+$ MuSCs in RGD-functionalized 4% 20-kDa hydrogels cross-linked using either a protease-degradable peptide (GCRDVPMSMRGGDRCG; protease-sensitive) or protease-insensitive hexa(ethylene glycol) dithiol (protease-insensitive). MuSCs cultured in protease-degradable hydrogels formed robust myogenic colonies after 4 days in culture, whereas we observed minimally viable MuSCs and no myogenic colonies in the protease-insensitive hydrogels (Fig. 3, A and B). A single MuSC encapsulated in protease-sensitive matrix readily degraded the surrounding matrix to proliferate and form a robust myogenic colony over time, whereas a MuSC in nondegradable, protease-insensitive matrix remained entrapped and unable to proliferate over time (Fig. 3C). Furthermore, the mechanical properties of protease-sensitive hydrogels containing MuSC declined with time in culture (Fig. 3D), and the calculated mesh size (Fig. 3E) increased over culture time. As expected, the mechanical properties and mesh size of MuSC-laden protease-insensitive cells remained relatively constant over time in culture. These results indicate that use of protease-degradable cross-linking peptides, which enable on-demand degradation of the cellular microenvironment, is essential for MuSC survival and proliferation in vitro within these synthetic niches.

Synthetic matrix supports higher MuSC proliferation potential than natural matrices

Collagen gels are commonly used as a natural extracellular matrix for cell culture in 3D. To determine how the engineered PEG-4MAL hydrogels perform in supporting MuSC function in comparison to collagen gels as a benchmark material, we encapsulated freshly isolated GFP$^+$ MuSCs in either RGD-functionalized 4% 20-kDa hydrogels cross-linked using protease-degradable peptides or type I collagen gels (2.7 mg ml^{-1}; storage modulus, 70 ± 16 Pa). Myogenic colonies formed after 4 days of culture were significantly larger in the PEG-4MAL synthetic hydrogels compared to collagen gels ($P < 0.0001$; Fig. 4, A and B). Despite the significant size differences in myogenic colonies formed in the PEG-4MAL hydrogels and collagen gels, we observed no differences in cell proliferation on day 4 of culture ($P > 0.05$; Fig. 4, C and D). However, assessment of dead cells at 1 day after encapsulation revealed that cell viability is significantly lower in collagen gels compared to the PEG-4MAL hydrogels ($P < 0.0001$; Fig. 4, E and F, and fig. S6A). We attribute the larger myogenic colonies formed in the PEG-4MAL hydrogels to higher cell viability upon encapsulation. To eliminate potential effects of material stiffness on myogenic colony formation in 3D, we cultured MuSCs in either type I collagen gel (2.7 mg ml^{-1}) or RGD-functionalized 2.8% 20-kDa PEG-4MAL hydrogels cross-linked with protease-degradable peptides, which exhibit similar storage modulus as type I collagen gel (2.7 mg ml^{-1}; fig. S6B). Despite comparable mechanical properties, myogenic colonies formed in 2.8% PEG-4MAL hydrogels were significantly

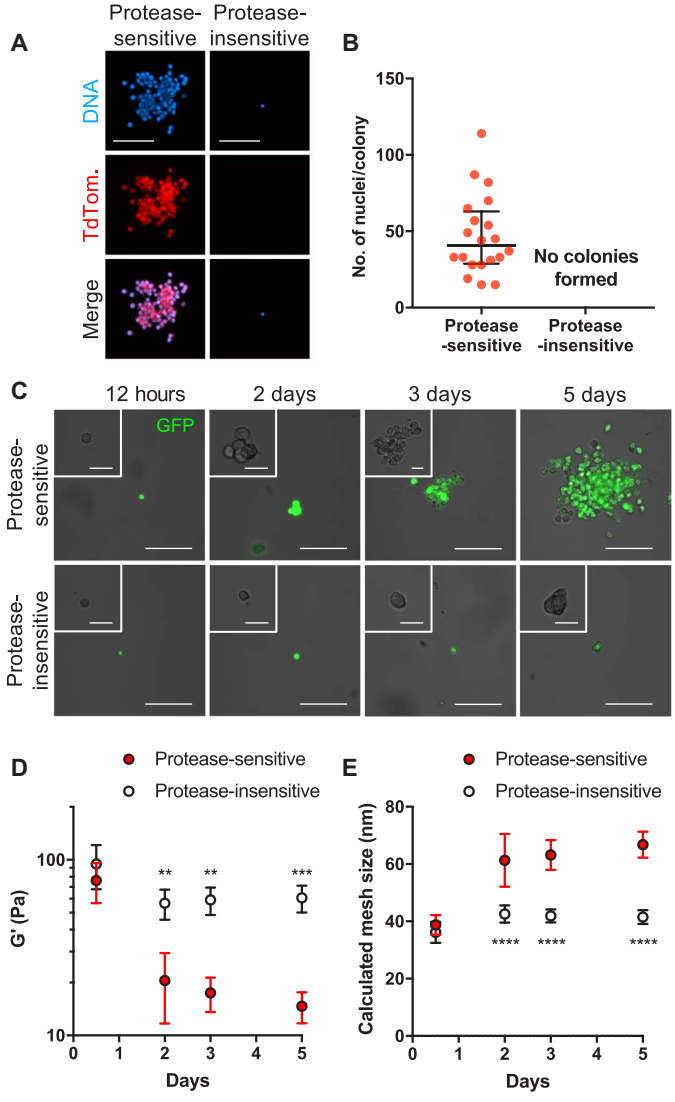

Fig. 3. Protease degradability of the hydrogel is essential for MuSC proliferation. (**A**) Representative *z*-projections of MuSCs cultured in RGD-functionalized hydrogels synthesized with protease-sensitive and protease-insensitive cross-linkers (day 4). Scale bars, 100 μm. TdTom., TdTomato. (**B**) Quantification of myogenic colonies. Median ± interquartile range. $n = 20$. (**C**) Representative myogenic colony formation over time in protease-sensitive hydrogel and in protease-insensitive hydrogels over 5 days. Scale bars, 50 μm (main images) and 10 μm (insets). (**D**) Storage modulus and (**E**) mesh size of protease-sensitive and protease-insensitive hydrogels over 5 days. $^{**}P < 0.01$, $^{***}P < 0.001$, and $^{****}P < 0.0001$ versus time-matched protease-sensitive hydrogels via two-way ANOVA with Sidak's test. $n = 4$ hydrogels per time point. Mean ± SD.

Downloaded from http://advances.sciencemag.org/ on July 5, 2019

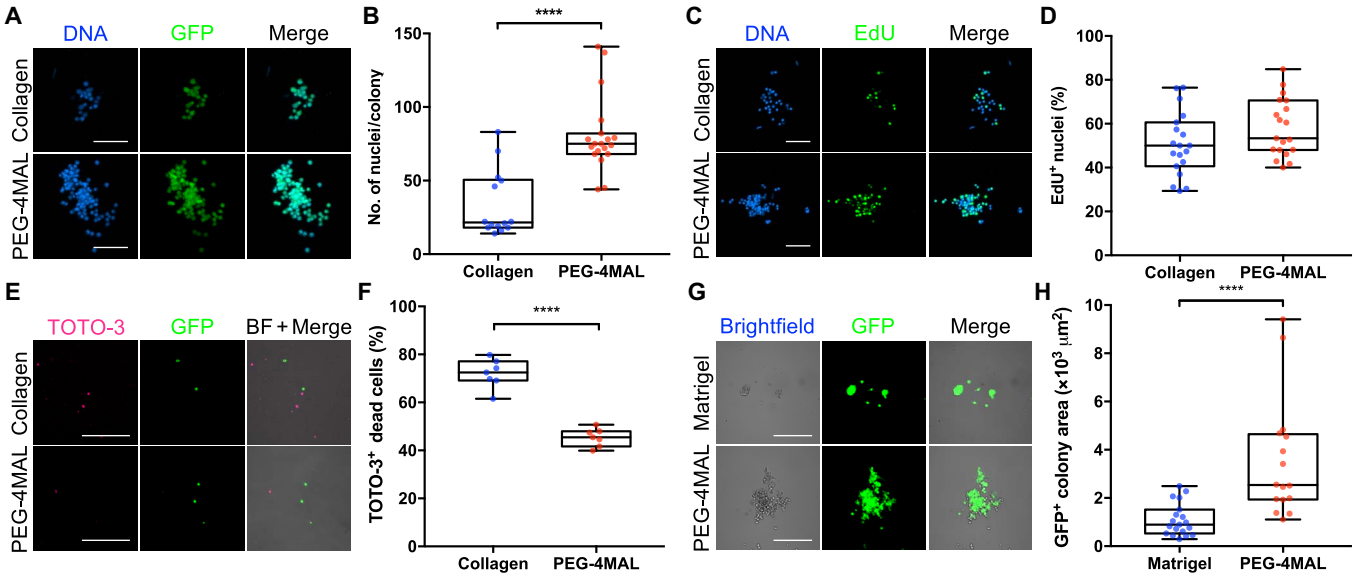

Fig. 4. Synthetic matrix supports higher MuSC proliferation potential than natural matrices. (**A**) Representative *z*-projections of myogenic colonies formed in 4% PEG-4MAL and collagen gels (2.7 mg ml^{-1}; day 4). Scale bars, 100 μm. (**B**) Quantification of myogenic colony size. n = 14 to 19 colonies. ****P < 0.0001 via two-tailed Mann-Whitney U test. (**C**) Representative *z*-projections of EdU-labeled myogenic colonies formed in 4% PEG-4MAL and collagen gels (2.7 mg ml^{-1}; day 4). Scale bars, 100 μm. (**D**) Quantification of EdU$^+$ nuclei. n = 19 colonies. P = 0.11 via unpaired two-tailed t test. (**E**) Representative *z*-projections of GFP$^+$ MuSCs 1 day after encapsulation in 4% PEG-4MAL and collagen gels (2.7 mg ml^{-1}). BF, bright field. Scale bars, 100 μm. (**F**) Quantification of TOTO-3$^+$ dead MuSCs 1 day after encapsulation. n = 7 hydrogels. ****P < 0.0001 via unpaired two-tailed t test. (**G**) Representative images of GFP$^+$ MuSCs 4 days after encapsulation in 4% PEG-4MAL and Matrigel. Scale bars, 100 μm. (**H**) Quantification of GFP$^+$ myogenic colony area 4 days after encapsulation. n = 16 to 19 colonies. ****P < 0.0001 via two-tailed Mann-Whitney U test.

greater than colonies formed in collagen gel (2.7 mg ml^{-1}; fig. S6, C and D). This result suggests that other biophysical and biochemical differences, such as cell binding site (type and density), material microstructure and function, and transport properties, regulate the differences in MuSC function between these biomaterial systems.

In the context of skeletal muscle, Matrigel may be a more appropriate naturally derived matrix for myogenic cell culture, as a major constituent of Matrigel is laminin. To assess MuSC function in comparison to Matrigel as an additional benchmark material, we encapsulated freshly isolated GFP$^+$ MuSCs in either RGD-functionalized 4% 20-kDa hydrogels cross-linked with protease-degradable peptides or Matrigel (storage modulus, 25.2 ± 7.8 Pa). After 4 days of culture, we observed significantly larger myogenic colonies in the PEG-4MAL synthetic hydrogel compared to Matrigel (P < 0.0001; Fig. 4, G and H). Furthermore, myogenic colonies formed in Matrigel were morphologically rounder and closely clustered (Fig. 4G). Although Matrigel is an appropriate reference material, it is important to highlight limitations associated with Matrigel. Matrigel is generated from the Engelbreth-Holm-Swarm sarcoma that is rich in undefined extracellular matrix proteins. As a result, Matrigel is subjected to significant lot-to-lot variability in terms of composition and mechanical properties and poses potential risk of pathogen transfer and immunogenicity, significantly limiting its clinical translation. Nonetheless, the results collectively demonstrate that the engineered synthetic matrix supports higher MuSC proliferation potential than collagen gels and Matrigel.

Synthetic matrix boosts engraftment in dystrophic muscle trauma

Acute muscle trauma imparts significant burden on the endogenous MuSC population to regenerate the damaged muscle (*25*–*27*), and the regenerative potential of muscle is further challenged when the normal mechanisms of muscle regeneration and homeostasis are chronically dysregulated (*1*). For instance, DMD muscles lacking dystrophin exhibit reduced mechanical integrity and are prone to sarcolemma rupture upon repeated contraction. Moreover, dystrophin-deficient MuSCs exhibit abnormal mitosis and asymmetric division capacity (*14*, *15*), exacerbating the detrimental consequences of muscle injury. Transplantation of MuSCs stimulates muscle regeneration through cellular engraftment (*28*); however, cell delivery via direct injection poses several challenges at the translational level, including poor cell survival and limited applicability to traumatic injuries. To this end, we applied the bioengineered synthetic matrix to deliver MuSCs to the superficially injured TA muscles of *mdx-4CV* mice, which exhibit chronic muscle degeneration and regeneration. We hypothesized that MuSCs delivered within the engineered PEG-4MAL hydrogel, which supports survival, activation, and proliferation, would migrate into the host muscle, resulting in enhanced cellular engraftment. The PEG-4MAL hydrogel system enables in situ polymerization and direct integration to host tissue through thiol-presenting tissue and maleimide functional groups to improve in vivo cell retention and delivery, thus providing a major advantage over other synthetic and natural materials (*50*). TA muscles of recipient *mdx-4CV* mice (13 to 19 weeks old) were injured by exposing the muscle surface to a liquid nitrogen–cooled probe before transplantation (Fig. 5A). A cryo-injury model was selected because it induces more localized injury compared to other commonly used models, such as cardiotoxin and notexin injections, through ablation of myofibers and mononuclear cells at the site of injury and necessitates MuSCs to migrate in from the noninjured sites (*57*, *58*). To evaluate the effects of PEG-4MAL polymer density on MuSC engraftment in vivo, we delivered freshly isolated β-actin GFP$^+$/luciferase$^+$ MuSCs encapsulated in 3% 20-kDa PEG-4MAL hydrogels containing 1.0 mM RGD, 6% 20-kDa PEG-4MAL hydrogels containing 1.0 mM RGD, or suspended

Downloaded from http://advances.sciencemag.org/ on July 5, 2019

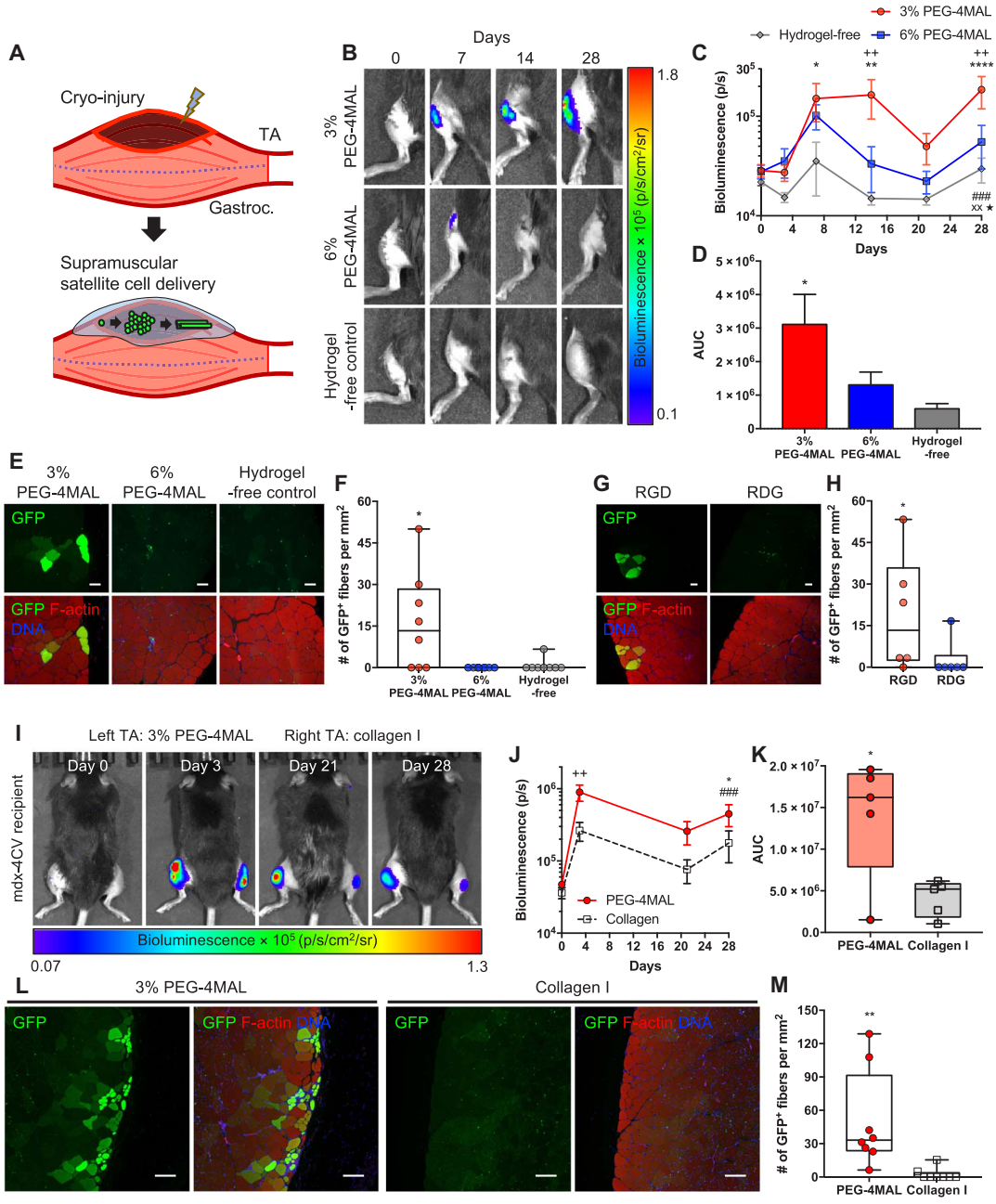

Fig. 5. Synthetic matrix enhances engraftment in dystrophic muscle trauma. (**A**) Schematic of injury and cell delivery. We applied cryo-injury on the surface of TA muscle. We supramuscularly delivered freshly isolated MuSCs in media (hydrogel-free) or encapsulated in hydrogel. Gastroc., gastrocnemius muscles. (**B**) Representative IVIS images of *mdx-4CV* mouse hindlimbs treated with cell-laden 3% 20-kDa PEG-4MAL, 6% 20-kDa PEG-4MAL, or media (12,500 MuSCs per TA). (**C**) Quantification of bioluminescence over time. Mean ± SEM. $n = 8$ per condition. $^{*}P < 0.05$, $^{**}P < 0.01$, and $^{****}P < 0.0001$ versus hydrogel-free via Tukey's test within time. $^{++}P < 0.01$ versus 6% PEG-4MAL via Tukey's test within time. $^{*}P < 0.05$ for interactions, $^{xx}P < 0.01$ for biomaterials effect, and $^{###}P < 0.001$ for time effect via two-way repeated-measures ANOVA. (**D**) Quantification of area under the bioluminescence curve (AUC). Mean ± SEM. $n = 8$ per condition. $^{*}P < 0.05$ versus hydrogel-free via one-way ANOVA with Tukey's test. (**E**) Representative cross sections of TA muscles treated with cell-laden 3% 20-kDa PEG-4MAL, 6% 20-kDa PEG-4MAL, or media on day 28 after transplantation. Scale bars, 50 μm. (**F**) Quantification of GFP^{+} fibers per square millimiter. $n = 8$ per condition. $^{*}P < 0.05$ versus all groups via Kruskal-Wallis with Dunn's test. (**G**) Representative cross sections of TA muscles treated with cell-laden 3% 20-kDa PEG-4MAL functionalized with RGD or RDG peptides at day 28 after transplantation (12,500 MuSCs per TA). Scale bars, 50 μm. (**H**) Quantification of GFP^{+} fibers per square millimeter. $n = 6$ per condition. $^{*}P < 0.05$ via two-tailed Mann-Whitney *U* test. (**I**) Representative IVIS images of MuSC-transplanted *mdx-4CV* mice. TA muscles were cryo-injured, and 20,000 MuSCs were delivered to the injured TA muscles in either PEG-4MAL hydrogel (left) or collagen gel (2.7 mg ml^{-1}; right). (**J**) Quantification of bioluminescence over time. Mean ± SEM. $n = 5$ per condition. $^{++}P < 0.01$ within time via Sidak's test. $^{*}P < 0.05$ for interactions and biomaterials effect via two-way repeated-measures ANOVA. $^{###}P < 0.05$ for time effect via two-way repeated-measures ANOVA. (**K**) Quantification of AUC. $n = 8$ per condition. $^{*}P < 0.05$ via two-tailed paired *t* test. (**L**) Representative cross sections of TA muscles treated with 50,000 MuSCs in either PEG-4MAL or collagen gel (2.7 mg ml^{-1}). Scale bars, 100 μm. (**M**) Quantification of engrafted GFP^{+} fibers per square millimeter. $n = 8$ per condition. $^{**}P < 0.01$ via two-tailed Wilcoxon matched-pairs signed-rank test.

Downloaded from http://advances.sciencemag.org/ on July 5, 2019

in media (hydrogel-free) atop the injured TA muscles immediately after muscle injury (Fig. 5A). Both PEG-4MAL gels were cross-linked using protease-degradable peptides. We elevated and sustained the bioluminescence signal of MuSCs delivered in 3% PEG-4MAL hydrogels through day 28 after transplantation compared to hydrogel-free condition ($P < 0.01$ over time and $P < 0.05$ on day 28; Fig. 5, B and C). Analysis of the area under the bioluminescence curve further substantiated this observation ($P < 0.05$; Fig. 5D). MuSCs delivered in 3% PEG-4MAL hydrogels successfully differentiated and formed GFP$^+$ fibers, whereas MuSCs delivered in 6% PEG-4MAL hydrogels or media alone did not engraft ($P < 0.05$; Fig. 5, E and F). Collectively, the results indicate that MuSCs delivered in 3% PEG-4MAL hydrogels directly on top of acutely injured dystrophic TA muscles support in vivo retention, survival, and proliferation and promote cellular engraftment into the injured host muscle.

We next examined the importance of the RGD adhesive peptide in the delivery hydrogel vehicle on MuSC engraftment. We compared GFP$^+$ MuSC transplantation efficacy using 3% PEG-4MAL hydrogels cross-linked with protease-sensitive peptides and functionalized with either 1.0 mM RGD or 1.0 mM scrambled RDG in the cryo-injured TA muscles of *mdx-4CV* mice. We observed a significantly higher number of GFP$^+$ fibers in the RGD-presenting hydrogel group compared to the scrambled RDG-presenting hydrogel group on day 28 after transplantation ($P < 0.05$; Fig. 5, G and H), demonstrating that presentation of RGD cell-adhesive peptide with the delivery vehicle is required for the engraftment of delivered MuSCs.

To directly compare MuSC transplantation efficacy of the engineered PEG-4MAL hydrogels to collagen gels, we monitored the bioluminescence signal of MuSCs delivered to injured muscle using either RGD-presenting 3% PEG-4MAL hydrogels cross-linked with protease-sensitive peptides or collagen gels (2.7 mg ml^{-1}) over time. MuSCs delivered using the PEG-4MAL hydrogels exhibited a significantly higher overall bioluminescence signal compared to collagen over the course of 28 days ($P < 0.05$; Fig. 5, I and J). Further analysis of the area under the bioluminescence curve substantiated that MuSCs delivered using PEG-4MAL hydrogels resulted in significantly higher engraftment than MuSCs delivered using collagen gels ($P < 0.05$; Fig. 5K), indicating superior performance of the PEG-4MAL hydrogel compared to collagen gels for delivery of MuSCs to injured TA muscles.

The engraftment potential is strongly dependent on the number of MuSCs delivered (*19*, *29*, *55*). To demonstrate the feasibility of achieving a higher number of engrafted fibers using the engineered PEG-4MAL hydrogels, we delivered approximately 50,000 freshly isolated GFP$^+$ MuSCs to the cryo-injured TA muscles of *mdx-4CV* mice. Delivery of MuSCs in 3% PEG-4MAL hydrogels resulted in robust engraftment 28 days after transplantation, where the mean number of GFP$^+$ fibers increased significantly (~15 to 50 fibers/mm^2) by increasing the donor cell quantity (Fig. 5, L and M). Delivery of MuSCs using collagen gel resulted in minimal engraftment (Fig. 5, L and M), further demonstrating the efficacy of the engineered PEG-4MAL hydrogels.

Synthetic matrix boosts MuSC engraftment in aged muscle trauma

Aged skeletal muscles exhibit impaired regenerative capacity upon injury (*2*). To confirm that aged muscles exhibit diminished regeneration upon superficial cryo-injury compared to young muscles, we subjected young (4 months old) and aged (22 months old) muscles to cryo-injury, as described above, and assessed their native endogenous regeneration. Young (4 months old) TA muscle regenerated to tissue comparable to native uninjured TA muscle by day 14 after injury, whereas aged (22 months old) TA muscle did not completely regenerate by day 14 after injury, as indicated both by the smaller fiber cross-sectional area and by the higher presence of centrally localized myonuclei ($P < 0.0001$; Fig. 6, A and B). To test whether the engineered PEG-4MAL hydrogel can also promote MuSC engraftment in injured aged muscle, we delivered freshly isolated β-actin GFP$^+$/luciferase$^+$ MuSCs encapsulated in 3% 20-kDa PEG-4MAL hydrogels containing 1.0 mM RGD and cross-linked with protease-degradable peptides or suspended in media (hydrogel-free) to the supramuscular locus of the cryo-injured TA muscles of aged mice (23 months old). Delivery of MuSCs using the PEG-4MAL hydrogel resulted in a progressive increase in the bioluminescence signal up to 7 days after transplantation, and this signal was sustained through day 28 after transplantation (Fig. 6, C and D). In contrast, MuSCs delivered without the hydrogel resulted in no change in the bioluminescence signal over time, and this signal was significantly lower than the signal for the hydrogel group ($P < 0.05$; Fig. 6, C to E). Consistent with these results, we observed increased numbers of GFP$^+$ fibers, indicative of transplanted cell engraftment, for muscles treated with MuSCs delivered within PEG-4MAL gels, whereas we observed no GFP$^+$ fibers for muscles treated with MuSCs without the hydrogel carrier (Fig. 6F). These results show that PEG-4MAL hydrogel promotes donor MuSC retention, survival, proliferation, and engraftment in injured aged muscle.

DISCUSSION

Here, we engineered a synthetic hydrogel that promotes MuSC survival, proliferation, and differentiation in 3D culture. Furthermore, we demonstrated that the engineered PEG-4MAL hydrogel can be used as a delivery vehicle to transplant MuSCs to injured skeletal muscles that exhibit dysregulated homeostasis and regeneration, such as in aging and muscular dystrophy. This biomaterial platform offers a unique advantage for delivering cells to traumatically injured muscles with disrupted structural tissue integrity, as the maleimide functional groups of the PEG-4MAL system react with thiol-containing molecules and tissues to form covalent bonds via Michael-type addition under physiologic conditions, and offers the ability to firmly integrate the cell-encapsulated hydrogel to biological tissues (*50*). The engineered hydrogel is based solely on synthetic materials, which offers major advantages over naturally derived hydrogels including collagen and Matrigel. Synthetic matrices are minimally susceptible to lot-to-lot variations and pathogen transfer and thus are more suitable for translating the technology to the clinics. Moreover, the biophysical and biochemical properties of the synthetic matrix can be modulated in a highly precise and controlled manner, enabling identification of key cellular niche parameters for directing cell function.

To design a synthetic matrix that enhances MuSC function (that is, survival, activation, proliferation, and differentiation) for cell delivery applications, we reasoned that key factors found in the native MuSC niche must be incorporated into an otherwise biologically inert PEG-based hydrogel. MuSCs reside in between muscle fiber sarcolemma and its surrounding laminin-rich basal lamina matrix. Upon injury, fibronectin content in the basal lamina transiently increases and induces MuSC expansion (*59*). In addition, fibronectin has been identified as a preferred adhesion substrate for MuSCs, where fibronectin targets β1 integrin and synergistically acts with FGF-2 to activate common downstream signaling through the mitogen-activated protein kinase ERK (extracellular signal–regulated kinase) and protein kinase B for

Downloaded from http://advances.sciencemag.org/ on July 5, 2019

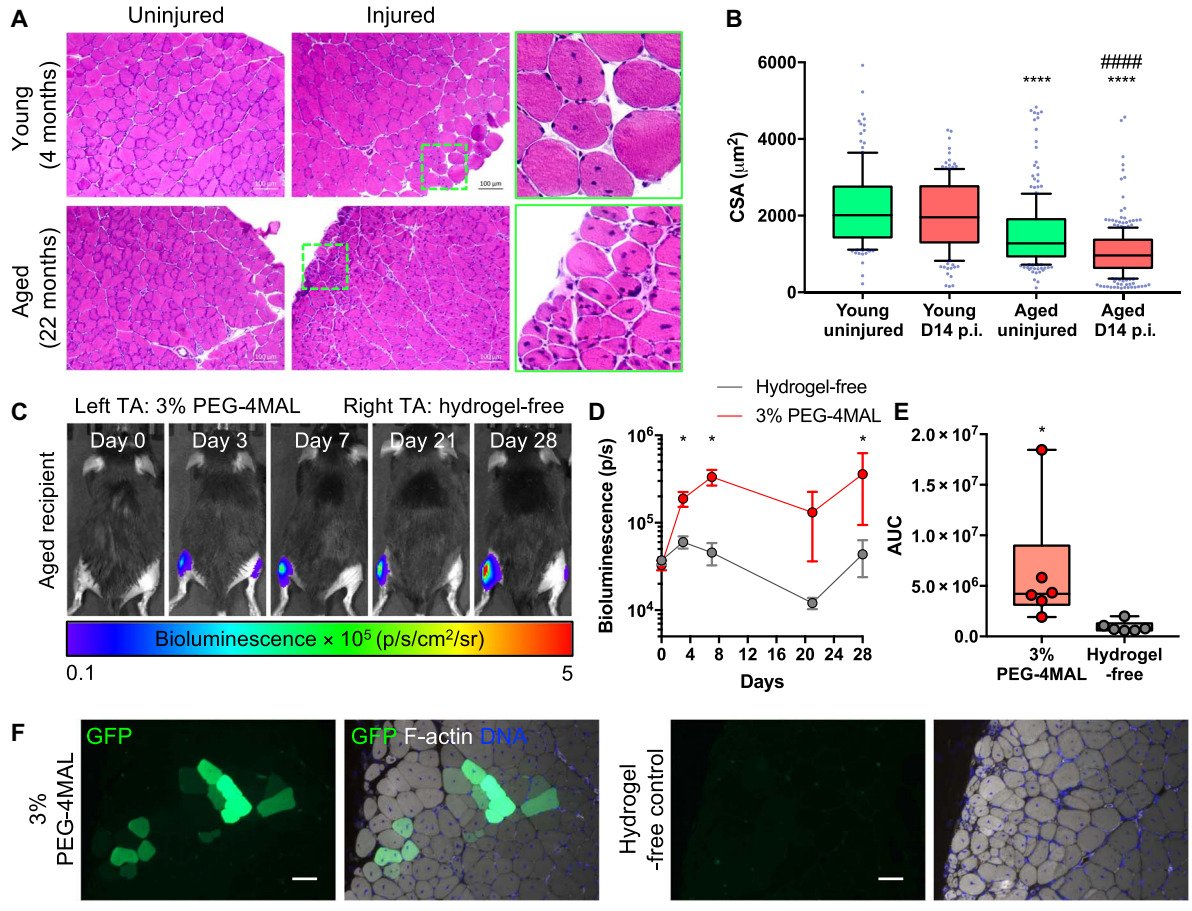

Fig. 6. Synthetic matrix enhances engraftment in aged muscle trauma. (**A**) Hematoxylin and eosin images of young (4 months) and aged (22 months) TA muscles. Muscles were cryo-injured, and endogenous regeneration was assessed on day 14 (D14). (**B**) Quantification of cross-sectional area (CSA). Box-and-whiskers plot with 10 to 90 percentile whiskers. We measured ≥138 fibers. p.i., postinjury. $^{****}P < 0.0001$ versus young uninjured and young D14 postinjury; $^{\#\#\#\#}P < 0.0001$ versus aged uninjured via one-way ANOVA with Dunn's test. (**C**) Representative IVIS images of aged mice (23 months). TA muscles were cryo-injured, and 20,000 MuSCs encapsulated in PEG-4MAL hydrogel (left) or suspended in media (right) were transplanted. (**D**) Quantification of bioluminescence over time. Mean ± SEM. $n = 6$ per condition. $^{*}P < 0.05$ via two-tailed Wilcoxon matched-pairs signed-rank test within time. (**E**) Quantification of AUC. $n = 6$ per condition. $^{*}P < 0.05$ via two-tailed Wilcoxon matched-pairs signed-rank test. (**F**) Cross sections of TA muscles at day 28 after transplantation. Scale bars, 50 μm.

MuSC expansion and self-renewal (*52*, *60*). Here, we showed that the RGD peptide, positioned within the cell-binding region of fibronectin, laminin, vitronectin, and collagen types I and IV (*61*), is necessary to promote primary MuSC survival, expansion, and differentiation within the synthetic hydrogel. Whereas the RGD peptide has been shown to promote C2C12 and primary myoblast adhesion, proliferation, and differentiation (*49*, *62*), the effect of the RGD peptide as a bioactive cell-adhesive ligand for quiescent and activated MuSC function has not been established previously. RGD binds β1 integrin and β3 integrin (*61*), which are critical for MuSC expansion and differentiation (*54*, *60*), respectively. Binding of RGD to MuSC integrins also likely promotes cell survival through inhibition of anoikis (Fig. 1, H and I). With determination of the appropriate biophysical parameters and incorporation of on-demand matrix degradation capability, we achieved high levels of survival and proliferation of MuSCs (Figs. 2 and 3 and fig. S5). Although it is outside the scope of the current study, there is potential to further engineer this platform to promote quiescence and self-renewal in combination with a quiescence medium (*34*) and presentation of asymmetrical and/or spatiotemporal cues for ex vivo expansion of MuSCs.

We also established a biomaterial-mediated cell delivery strategy for treating skeletal muscle trauma involving severe lacerations, burns, and surgical resections, where intramuscular injections may not be directly applicable. Although healthy skeletal muscles have remarkable regenerative potential, their regenerative capacity becomes severely limiting with trauma, and the problem is further exacerbated in conditions with impaired muscle regeneration, such as aging and muscular dystrophy. To demonstrate the feasibility of supramuscular delivery of MuSCs in these potential clinical situations, we used cryo-injured dystrophic and aged muscles as in vivo proof-of-concept systems in this study. Delivery of freshly isolated MuSCs using the engineered PEG-4MAL hydrogel to the supramuscular locus of the injured muscle promoted in vivo cell survival, retention, proliferation, and engraftment in both aging and muscular dystrophy contexts compared to collagen gels and hydrogel-free controls, demonstrating the versatility of this platform to treat different muscle conditions. Note that here, we delivered 12,500 to 20,000 freshly isolated MuSCs per nonirradiated, immunocompetent TA muscle (Figs. 5, B to K, and 6). The engraftment rate and degree of engraftment are strongly dependent on the number of MuSCs delivered

Downloaded from http://advances.sciencemag.org/ on July 5, 2019

(*19*, *29*, *55*), and thus, this biomaterial-mediated cell delivery strategy could be further potentiated by increasing the donor cell quantity. We demonstrate that increasing the donor cell number significantly enhances cell engraftment (Fig. 5, L and M). For translation of cell-based technologies to the clinic, challenges associated with sourcing and manufacturing MuSCs need to be overcome through development of ex vivo expansion technologies and generation of induced pluripotent stem cell–derived myogenic progenitor cells (*34*, *55*, *63*). Finally, it would also be important to further extend the current strategy to more severe injury models, such as volumetric muscle loss where the muscle architecture and function are irreversibly compromised. Nonetheless, the biomaterial presented here sets a promising foundation to deliver cells and biologics to augment skeletal muscle regeneration upon trauma.

To overcome inherent limitations and challenges presented by direct cell delivery, numerous natural and synthetic biomaterials have been developed for cell transplantation to skeletal muscle (*34*–*45*, *64*). Although biomaterial-assisted cell delivery critically mitigates direct cell delivery challenges and improves therapeutic outcomes, many of the previous investigations focused on delivering cultured myoblasts (*36*–*38*, *40*, *42*), where their engraftment potency is severely restricted compared to quiescence MuSCs (*33*, *34*, *39*, *55*). Quiescent MuSCs lose potency within 7 days of expansion in vitro and result in poor survival and engraftment in the host muscle upon transplantation (*34*, *55*), significantly limiting the translational potential. To further address these challenges and improve therapeutic outcomes, natural and natural-synthetic composite hydrogels have been engineered to facilitate the delivery of quiescent MuSCs and demonstrated positive effects in promoting MuSC engraftment (*34*, *35*, *39*). More recently, synthetic scaffolds for MuSC delivery have been developed to circumvent potential limitations associated with naturally derived materials (*64*), such as susceptibility to lot-to-lot variations and pathogen transfer. However, previous evaluations of biomaterials for quiescent and activated MuSC delivery used preirradiated and immunocompromised [for example, NOD/Scid (nonobese diabetic/severe combined immunodeficient), RAG2 (recombination activating gene 2)/γ-chain knockout, NSG (NOD/Scid/γ), and athymic nude] mice, diminishing the clinical applicability. For instance, engraftment of donor MuSCs in the presence of competent host MuSCs is more challenging (*65*). Furthermore, interactions between muscle and immune cells, as well as interactions between biomaterials and immune cells, critically dictate the regenerative and therapeutic outcomes of the muscle (*66*), and thus, contributions of the host MuSCs and immune system are important considerations at the translational level. Although it is difficult to directly compare the current data with previous investigations due to these inherent technical differences and commercial availability of previously reported materials, the current study provides important insights into enhancing the delivery of quiescent MuSCs using a fully synthetic matrix into nonirradiated, immunocompetent dystrophic, and aged skeletal muscles.

In summary, we present an innovative biomaterial-based strategy to support stem cell therapy for treating skeletal muscle injuries. This platform could be useful for treating acute trauma of craniofacial, extraocular, and limb muscles and addressing postoperative wounds arising from surgical tumor ablation and surgical interventions of muscular dystrophies. With concurrent advancement of effective MuSC sourcing, through ex vivo MuSC manipulation and induced pluripotent stem cell technologies, this platform could be further developed for applications in treatment of large muscle trauma, including laceration, severe burn, and volumetric muscle loss in combination with spatiotemporal delivery of proregenerative biologics and emergent gene editing technologies.

MATERIALS AND METHODS

Animals

C57Bl/6, *B6Ros.Cg-DMD$^{mdx\text{-}4CV}$/J*, *FVB-Tg(CAG-luc,-GFP)L2G85Chco/J*, *B6.Cg-Gt(ROSA)$^{26Sortm14(CAG\text{-}TdTomato)Hze}$/J*, and *B6.C-Tg(CMV-cre)1Cgn/J* mice were obtained from the Jackson Laboratory. *C57Bl/6-β-actin-EGFP* mice were provided by A. Wagers, Harvard University. *R26R-TdTomato/CMV-cre* mice were acquired by crossing *B6.Cg-Gt(ROSA)$^{26Sortm14(CAG\text{-}TdTomato)Hze}$/J* and *B6.C-Tg(CMV-cre)1Cgn/J* mice. *CAG-luc-Ka-β-actin-EGFP* mice were acquired by crossing *FVB-Tg(CAG-luc,-GFP)L2G85Chco/J* and *C57Bl/6-β-actin-EGFP* mice. Both male and female mice were used in this study in a randomized manner. Mice were housed, aged, and/or bred in the Physiological Research Laboratory Animal Facility of Georgia Tech. All animal procedures were conducted under the approval of the Institutional Animal Care and Use Committee of Georgia Tech.

MuSC isolation

MuSCs were isolated as described previously, with minor modifications (*28*). Hindlimb muscles were dissected from 2- to 4-month old mice, minced, and digested in Dulbecco's modified Eagle's medium (DMEM) containing type II collagenase (0.2%; Worthington Biochemical Corp.) and dispase II (2.5 U ml^{-1}; Roche) for 90 min at 37°C. The digest solution containing the muscles was triturated every 30 min using a donor bovine serum (DBS)–coated serological pipette. A two-part volume of 20% DBS in F10 media was added to the digested solution and filtered through a 70-μm cell strainer. The solution was centrifuged (300*g*) for 5 min at 4°C to yield cell pellets. Cell pellets were washed using 2% DBS in Hanks' balanced salt solution (HBSS; 300*g* centrifugation for 5 min at 4°C) and resuspended in 2% DBS in HBSS. Cells were incubated with a cocktail of primary antibodies (1:100) consisting of phycoerythrin (PE)–conjugated anti-mouse β1 integrin (CD29, 20.0%; BioLegend), anaphase-promoting complex–conjugated anti-mouse Sca1 (13.3%, v/v; BioLegend), CD45 (13.3%; BioLegend), CD11b (13.3%; BioLegend), Ter119 (13.3%; BioLegend), and biotinylated anti-mouse CD184 (CD184, 26.8%; BD Pharmingen) in 2% DBS in HBSS for 30 min on ice. Cells were washed in 2% DBS in HBSS and subsequently incubated with secondary antibody (Streptavidin PE-Cy7; 1:100; eBioscience) for 20 min on ice. Stained cells were washed as above, and propidium iodide$^-$, Sca1$^-$, CD45$^-$, CD11b$^-$, Ter119$^-$, β1 integrin$^+$, and CXCR4$^+$ cells were sorted via fluorescence-activated cell sorting, as described previously (BD FACSAria III Cell Sorter) (*28*).

Hydrogel synthesis, cell encapsulation, and culture

Four-arm PEG-4MAL macromer (molecular weight, 22,000 or 10,000; Laysan Bio) was dissolved in 1× phosphate-buffered saline (PBS) containing 10 mM Hepes (pH 7.4). Cell adhesive peptides (GRGDSPC, GRDGSPC, CGGEGYGEGYIGSR, and CGGKAFDITYVRLKF; >95% purity; GenScript) were dissolved in 1× PBS containing 10 mM Hepes and added to PEG-4MAL solution to produce functionalized PEG-4MAL precursors. Freshly isolated MuSCs were then added to the solution containing functionalized PEG-4MAL precursors. To synthesize cell-encapsulated hydrogels, the solution containing functionalized PEG-4MAL precursors and cells was mixed with protease-degradable cross-linking peptide (GCRDVPMSMRGGDRCG; GenScript) or non-degradable hexa(ethylene glycol) dithiol (Sigma-Aldrich) dissolved in 1× PBS containing 10 mM Hepes and subsequently polymerized at 37°C/5% CO_2 for 5 min before adding MuSC growth media (F10 containing 1% penicillin/streptomycin, 1% GlutaMAX, and 20% horse serum). Recombinant human FGF-2 (25 ng ml^{-1}; PeproTech) was supplemented

Downloaded from http://advances.sciencemag.org/ on July 5, 2019

daily. To prime the MuSCs to differentiate, the growth medium was replaced with differentiation media (DMEM containing 1% penicillin/streptomycin, 1% GlutaMAX, and 2% horse serum) on days 5 and 6 of culture. Cells were cultured in the differentiation media for an additional 4 days.

Cell encapsulation in collagen gel

Freshly isolated MuSCs (10,000 cells per gel) were added to the rat-tail collagen type I working solution consisting of 200 mM Hepes (10.4%, v/v), 10× DMEM (10.4%), 7.5% $NaHCO_3$ (5.2%), and collagen I (5 mg ml^{-1}; 54%; Rat Collagen I, lot # 30871G14, Culturex). Before adding cells, pH of the collagen working solution was adjusted by adding 1 M NaOH. pH-adjusted, cell-containing collagen solution was polymerized at 37°C/5% CO_2 for 30 min before adding MuSC growth media. Recombinant human FGF-2 (25 ng ml^{-1}) was supplemented daily.

Cell encapsulation in Matrigel

Freshly isolated MuSCs (10,000 cells; 2 of 10 parts) were added to the Matrigel (8 of 10 parts; phenol and lactose dehydrogenase-elevating virus–free; lot # 5075010, Corning). Cell-containing Matrigel was polymerized at 37°C/5% CO_2 for 45 min before adding MuSC growth media. Recombinant human FGF-2 (25 ng ml^{-1}) was supplemented daily.

In vitro cell staining and myogenic colony quantification

For EdU labeling, cells encapsulated in hydrogels were incubated in growth media containing 10 μM EdU for 6 hours. Hydrogels were fixed in 4% paraformaldehyde for 20 min and subsequently washed three times in 1× PBS. Cells within the hydrogels were blocked and permeabilized using blocking buffer [5% bovine serum albumin (BSA), 0.5% goat serum, and 0.5% Triton X-100 in 1× PBS] for 1 hour at room temperature. EdU detection was performed as per the manufacturer's instructions (Invitrogen). TUNEL staining and detection were performed as per the manufacturer's instructions (Invitrogen). Hydrogels were incubated with primary antibodies overnight at 4°C, washed three times in 1× PBS, incubated with secondary antibodies containing Hoechst (1:1000) overnight at 4°C, and washed again three times in 1× PBS. *z*-stack projection images were acquired using a confocal microscope (Nikon Eclipse Ti-E C2+). Myogenic colony morphology, size, and percent EdU^+ nuclei were automatically quantified using ImageJ and CellProfiler (*67*). Cell packing density was measured by segmenting the colony of interest, converting 4′,6-diamidino-2-phenylindole channel of a MuSC colony into a binary image (white pixel value, 255; black pixel value, 0) and subsequently determining the mean pixel value, where the resulting value ranges from 0 (less dense) to 255 (more dense). The mean pixel values were then normalized by dividing by 255 to obtain a cell packing density metric that ranges from 0 (less dense) to 1 (more dense). The fusion index was determined by taking the percentage of nuclei contained in multinucleated myotubes with at least two nuclei.

TOTO-3 iodide dead cell labeling

Freshly isolated β-actin–GFP^+ MuSCs were encapsulated in either PEG-4MAL or collagen gels and cultured in growth media overnight. TOTO-3 iodide (Invitrogen) was then added to the media at final concentration of 1 μM. Cells were incubated at 37°C/5% CO_2 for 30 min *z*-stack projection images were acquired using a confocal microscope (Nikon Eclipse Ti-E C2+) equipped with LiveCell system (Pathology Devices Live Cell) at 37°C/5% CO_2/50% relative humidity. TOTO-3^+ dead cells were quantified by taking the percentage of TOTO-3^+ nuclei over total cell number.

TaqMan reverse transcription polymerase chain reaction

Primary MuSCs were cultured in RGD- or RDG-presenting hydrogels in the growth media for 6 days and differentiated in the differentiation media for an additional 5 days. Hydrogels were mechanically homogenized, and RNA was extracted using TRIzol Reagent (Thermo Fisher Scientific). Quality and amount of RNA were assessed using NanoDrop (Thermo Fisher Scientific) at an absorbance at 260 and 280 nm. Complementary DNA (cDNA) was obtained using the High-Capacity cDNA Reverse Transcription Kit, as per the manufacturer's instructions (Thermo Fisher Scientific). Reverse transcription polymerase chain reaction was performed using TaqMan assay primers (*Myogenin*, *Desmin*, *Gapdh*, and β-*actin* probes) and TaqMan Fast Advanced Master Mix, as per the manufacturer's instructions (Thermo Fisher Scientific). C_t (cycle threshold) values of *Myogenin* and *Desmin* were normalized to the geometric mean of *Gapdh* and β-*actin* control genes. Fold differences were determined using $2^{-\Delta\Delta Ct}$.

Rheological testing and mesh size estimation

Hydrogels were casted in Sigmacote-treated (Sigma-Aldrich) cylindrical molds consisting of a glass slide and a silicone isolator. Upon gelation at 37°C, hydrogels were extracted and swelled in 1× PBS at 4°C overnight. Cell-containing hydrogels were synthesized and cultured in growth media, as described above for 12 hours and 2, 3, and 5 days. Fully swollen hydrogels were tested using a rheometer (MCR-302, Anton Paar; CP10-2) at 37°C. Frequency sweep (100 to 0.1 rad/s) was performed at a constant strain of 1%. G' and G'' were determined by averaging all data points acquired from 10 to 0.1 rad/s interval. Mesh size was estimated using the following equation

$$\xi = \left(\frac{G'A}{RT}\right)^{-\frac{1}{3}}$$

where G' is the storage modulus in Pa, A is the Avogadro's constant, R is the gas constant, and T is the temperature (*68*).

1D diffusion assay

Hydrogel was casted at one end of a glass capillary tube (outer diameter, 1 mm; inside diameter, 0.58 mm; World Precision Instruments) using an insulin syringe. Hydrogel-containing capillary tubes were placed in a 50-ml conical tube containing 1× PBS to fully swell overnight at 4°C. Alexa 555–labeled α-bungaroxin (8 kDa; 1:4 dilution in PBS; Thermo Fisher Scientific) was delivered to the other free end of the hydrogel-containing glass capillary tube. Samples were immediately placed in the temperature and humidity-controlled stage of an epifluorescence microscope (Zeiss Observer D1). Time-series images were acquired every 15 min for 3 hours at 37°C. Hydrogel boundary ($x = 0$) was defined by a region with an average raw intensity of 9.5 at $t = 0$. Change in the average intensity was quantified from $x = 0$ to 200 μm over the 3-hour assay period. To determine the diffusion coefficient (D), the data were fitted using the solution of Fick's second law

$$\varphi(x, t) = \varphi_0 \cdot \mathrm{erfc}\left(\frac{x}{2\sqrt{Dt}}\right)$$

Cryo-injury, MuSC transplantation, and injections

Mice were anesthetized by inhalation of isoflurane. The hair over TA muscle and gastrocnemius muscles was depilated to expose the skin. A small incision was made through the skin and fascia to expose the

Downloaded from http://advances.sciencemag.org/ on July 5, 2019

TA muscle. A liquid nitrogen–cooled metal probe was placed on the surface of the exposed TA muscle for 10 s to induce cryo-injury. Immediately upon muscle recovery, freshly isolated MuSCs were delivered on the locus of the injured TA muscle in suspension (2% DBS in HBSS), in rat-tail collagen type I (2.7 mg ml^{-1}; lot # 30871G14, Culturex), or in the bioengineered hydrogels. For the hydrogel-mediated delivery, the cell encapsulated hydrogel was casted directly on the surfaced of the injured TA muscle. The skin incision was carefully sutured (Vicryl Suture, Ethicon). All rodent survival procedures were performed using aseptic procedures.

Longitudinal bioluminescence imaging

Longitudinal bioluminescence imaging was performed using the IVIS SpectrumCT In Vivo Imaging System (PerkinElmer). Before imaging, mice were anesthetized by inhalation of isoflurane, and hindlimbs were depilated. Three hundred microliters of D-luciferin (4 mg; Promega) was injected intraperitoneally, and mice were imaged every 5 min up to 120 min to determine the maximal signal. The maximum signal was determined for each TA muscle and used for the subsequent analyses.

Tissue histology and immunostaining

Hindlimbs were harvested and fixed in 4% paraformaldehyde for 1 hour at room temperature and subsequently incubated in 30% sucrose overnight at 4°C. TA muscles were dissected and frozen in liquid nitrogen–cooled isopentane. Frozen muscles were sectioned to 10-μm thickness. Before antibody staining, tissue sections were blocked and permeabilized using blocking buffer (5% BSA, 0.5% goat serum, and 0.5% Triton X-100 in 1× PBS) for 1 hour at room temperature. Tissues for hematoxylin and eosin staining were prepared in a similar manner without the sucrose pretreatment.

GFP fiber quantification

For quantifying number of GFP^+ fibers in tissue sections, GFP channel images of anti-GFP antibody–stained tissue sections were acquired using an epifluorescence microscope (Zeiss Observer D1) or a confocal microscope (Zeiss LSM 700). Images were then converted to 8-bit, and automatic triangle-algorithm thresholds were applied using ImageJ. On the basis of the processed binary images, GFP^+ fibers were objectively identified and scored.

Antibodies and staining reagents

The following primary and secondary antibodies were used to stain cells and tissue sections for immunofluorescence in this study: Pax7 (1:50; Developmental Studies Hybridoma Bank), MyoD (1:200; C-20, Santa Cruz Biotechnology), myosin heavy chain (1:200; M4276, Sigma-Aldrich), desmin (1:200; H-76, Santa Cruz Biotechnology), Alexa Fluor 488–conjugated anti-GFP (1:250; A-21311, Thermo Fisher Scientific), Alexa Fluor 488 goat anti-mouse immunoglobulin G (IgG; 1:250; A-11029, Thermo Fisher Scientific), Alexa Fluor 488 goat anti-rabbit IgG (1:250; A-11034, Thermo Fisher Scientific), Alexa Fluor 555 goat anti-mouse IgG (1:250; A-21422, Thermo Fisher Scientific), and Alexa Fluor 555 goat anti-rabbit IgG (1:250; A-21424, Thermo Fisher Scientific). Alexa Fluor 555 phalloidin (1:50; Thermo Fisher Scientific) and Alexa Fluor 647 phalloidin (1:50; Thermo Fisher Scientific) were used to stain F-actin. Hoechst 33342 (1:1000; Thermo Fisher Scientific) and DRAQ5 (1:1000; Thermo Fisher Scientific) were used to counterstain cell nuclei.

Statistical analyses

Sample sizes were chosen on the basis of preliminary experiments to ensure adequate statistical power. Statistical analyses were performed using GraphPad Prism 7. Normality of data was tested using Shapiro-Wilk test and confirmed graphically via quantile-quantile plot. Outliers were detected using Grubb's test. Two-group comparisons were conducted using unpaired two-tailed *t* test or Mann-Whitney *U* test based on the data normality. For paired data, analyses were conducted using paired two-tailed Wilcoxon or *t* test based on data normality. For multiple group comparisons, one-way ANOVA with Tukey's post hoc tests or Kruskal-Wallis test with Dunn's post hoc tests was performed on the basis of data normality. Two-way ANOVA with Sidak's post hoc tests was performed for EdU^+ nuclei (%) data. Two-way repeated-measures ANOVA was performed on the longitudinal bioluminescence data to compare effects of biomaterial, time, and their interactions. The area under the curve was calculated in GraphPad Prism 7.

SUPPLEMENTARY MATERIALS

Supplementary material for this article is available at http://advances.sciencemag.org/cgi/content/full/4/8/eaar4008/DC1

Fig. S1. Isolated primary MuSCs are $Pax7^+$.
Fig. S2. RGD-presenting hydrogels promote MuSC activation and proliferation.
Fig. S3. RGD-presenting hydrogels promote MuSC differentiation.
Fig. S4. Pax7/MyoD expression of MuSCs in 4 and 6% 20-kDa PEG-4MAL hydrogels.
Fig. S5. 1D diffusion assay in PEG-4MAL hydrogels.
Fig. S6. Synthetic matrix supports higher MuSC proliferation potential than collagen gel.
Table S1. List of cell-adhesive synthetic peptides and their targets.
Movie S1. Differentiated myotubes in RGD hydrogels contract in vitro.

REFERENCES AND NOTES

1. A. E. Almada, A. J. Wagers, Molecular circuitry of stem cell fate in skeletal muscle regeneration, ageing and disease. *Nat. Rev. Mol. Cell Biol.* **17**, 267–279 (2016).
2. H. M. Blau, B. D. Cosgrove, A. T. V. Ho, The central role of muscle stem cells in regenerative failure with aging. *Nat. Med.* **21**, 854–862 (2015).
3. F. Oliva, A. G. Via, O. Kiritsi, C. Foti, N. Maffulli, Surgical repair of muscle laceration: Biomechanical properties at 6 years follow-up. *Muscles Ligaments Tendons J.* **3**, 313–317 (2014).
4. R. R. Kalyani, M. Corriere, L. Ferrucci, Age-related and disease-related muscle loss: The effect of diabetes, obesity, and other diseases. *Lancet Diabetes Endocrinol.* **2**, 819–829 (2014).
5. P. N. Siparsky, D. T. Kirkendall, W. E. Garrett Jr., Muscle changes in aging: Understanding sarcopenia. *Sports Health* **6**, 36–40 (2014).
6. J. D. Cross, J. R. Ficke, J. R. Hsu, B. D. Masini, J. C. Wenke, Battlefield orthopaedic injuries cause the majority of long-term disabilities. *J. Am. Acad. Orthop. Surg.* **19** (suppl. 1), S1–S7 (2011).
7. B. T. Corona, J. C. Rivera, J. G. Owens, J. C. Wenke, C. R. Rathbone, Volumetric muscle loss leads to permanent disability following extremity trauma. *J. Rehabil. Res. Dev.* **52**, 785–792 (2015).
8. J. F. Kragh Jr., S. J. Svoboda, J. C. Wenke, J. A. Ward, T. J. Walters, Suturing of lacerations of skeletal muscle. *J. Bone Joint Surg. Br.* **87**, 1303–1305 (2005).
9. B. Battiston, D. Ciclamini, J. B. Tang, Compound or specially designed flaps in the lower extremities. *Clin. Plast. Surg.* **44**, 287–297 (2017).
10. R. M. Garcia, D. S. Ruch, Free flap functional muscle transfers. *Hand Clin.* **32**, 397–405 (2016).
11. R. Sambasivan, R. Yao, A. Kissenpfennig, L. Van Wittenberghe, A. Paldi, B. Gayraud-Morel, H. Guenou, B. Malissen, S. Tajbakhsh, A. Galy, Pax7-expressing satellite cells are indispensable for adult skeletal muscle regeneration. *Development* **138**, 3647–3656 (2011).
12. C. Lepper, T. A. Partridge, C.-M. Fan, An absolute requirement for Pax7-positive satellite cells in acute injury-induced skeletal muscle regeneration. *Development* **138**, 3639–3646 (2011).
13. C. S. Fry, J. D. Lee, J. Mula, T. J. Kirby, J. R. Jackson, F. Liu, L. Yang, C. L. Mendias, E. E. Dupont-Versteegden, J. J. McCarthy, C. A. Peterson, Inducible depletion of satellite cells in adult, sedentary mice impairs muscle regenerative capacity without affecting sarcopenia. *Nat. Med.* **21**, 76–80 (2015).
14. N. A. Dumont, Y. X. Wang, J. von Maltzahn, A. Pasut, C. F. Bentzinger, C. E. Brun, M. A. Rudnicki, Dystrophin expression in muscle stem cells regulates their polarity and asymmetric division. *Nat. Med.* **21**, 1455–1463 (2015).

Downloaded from http://advances.sciencemag.org/ on July 5, 2019

15. A. Sacco, F. Mourkioti, R. Tran, J. Choi, M. Llewellyn, P. Kraft, M. Shkreli, S. Delp, J. H. Pomerantz, S. E. Artandi, H. M. Blau, Short telomeres and stem cell exhaustion model Duchenne muscular dystrophy in mdx/mTR mice. *Cell* **143**, 1059–1071 (2010).
16. S. Kuang, K. Kuroda, F. Le Grand, M. A. Rudnicki, Asymmetric self-renewal and commitment of satellite stem cells in muscle. *Cell* **129**, 999–1010 (2007).
17. A. Troy, A. B. Cadwallader, Y. Fedorov, K. Tyner, K. K. Tanaka, B. B. Olwin, Coordination of satellite cell activation and self-renewal by Par-complex-dependent asymmetric activation of p38α/β MAPK. *Cell Stem Cell* **11**, 541–553 (2012).
18. D. B. Gurevich, P. D. Nguyen, A. L. Siegel, O. V. Ehrlich, C. Sonntag, J. M. N. Phan, S. Berger, D. Ratnayake, L. Hersey, J. Berger, H. Verkade, T. E. Hall, P. D. Currie, Asymmetric division of clonal muscle stem cells coordinates muscle regeneration in vivo. *Science* **353**, aad9969 (2016).
19. B. D. Cosgrove, P. M. Gilbert, E. Porpiglia, F. Mourkioti, S. P. Lee, S. Y. Corbel, M. E. Llewellyn, S. L. Delp, H. M. Blau, Rejuvenation of the muscle stem cell population restores strength to injured aged muscles. *Nat. Med.* **20**, 255–264 (2014).
20. L. Liu, T. H. Cheung, G. W. Charville, B. M. C. Hurgo, T. Leavitt, J. Shih, A. Brunet, T. A. Rando, Chromatin modifications as determinants of muscle stem cell quiescence and chronological aging. *Cell Rep.* **4**, 189–204 (2013).
21. F. D. Price, J. von Maltzahn, C. F. Bentzinger, N. A. Dumont, H. Yin, N. C. Chang, D. H. Wilson, J. Frenette, M. A. Rudnicki, Inhibition of JAK-STAT signaling stimulates adult satellite cell function. *Nat. Med.* **20**, 1174–1181 (2014).
22. P. Sousa-Victor, S. Gutarra, L. García-Prat, J. Rodriguez-Ubreva, L. Ortet, V. Ruiz-Bonilla, M. Jardí, E. Ballestar, S. González, A. L. Serrano, E. Perdiguero, P. Muñoz-Cánoves, Geriatric muscle stem cells switch reversible quiescence into senescence. *Nature* **506**, 316–321 (2014).
23. J. D. Bernet, J. D. Doles, J. K. Hall, K. K. Tanaka, T. A. Carter, B. B. Olwin, p38 MAPK signaling underlies a cell-autonomous loss of stem cell self-renewal in skeletal muscle of aged mice. *Nat. Med.* **20**, 265–271 (2014).
24. B. E. Pollot, S. M. Goldman, J. C. Wenke, B. T. Corona, Decellularized extracellular matrix repair of volumetric muscle loss injury impairs adjacent bone healing in a rat model of complex musculoskeletal trauma. *J. Trauma Acute Care Surg.* **81**, S184–S190 (2016).
25. J. Song, M. R. Saeman, J. De Libero, S. E. Wolf, Skeletal muscle loss is associated with TNF mediated insufficient skeletal myogenic activation after burn. *Shock* **44**, 479–486 (2015).
26. X. Wu, T. J. Walters, C. R. Rathbone, Skeletal muscle satellite cell activation following cutaneous burn in rats. *Burns* **39**, 736–744 (2013).
27. C. S. Fry, C. Porter, L. S. Sidossis, C. Nieten, P. T. Reidy, G. Hundeshagen, R. Mlcak, B. B. Rasmussen, J. O. Lee, O. E. Suman, D. N. Herndon, C. C. Finnerty, Satellite cell activation and apoptosis in skeletal muscle from severely burned children. *J. Physiol.* **594**, 5223–5236 (2016).
28. M. Cerletti, S. Jurga, C. A. Witczak, M. F. Hirshman, J. L. Shadrach, L. J. Goodyear, A. J. Wagers, Highly efficient, functional engraftment of skeletal muscle stem cells in dystrophic muscles. *Cell* **134**, 37–47 (2008).
29. A. Sacco, R. Doyonnas, P. Kraft, S. Vitorovic, H. M. Blau, Self-renewal and expansion of single transplanted muscle stem cells. *Nature* **456**, 502–506 (2008).
30. D. Montarras, J. Morgan, C. Collins, F. Relaix, S. Zaffran, A. Cumano, T. Partridge, M. Buckingham, Direct isolation of satellite cells for skeletal muscle regeneration. *Science* **309**, 2064–2067 (2005).
31. J. K. Hall, G. B. Banks, J. S. Chamberlain, B. B. Olwin, Prevention of muscle aging by myofiber-associated satellite cell transplantation. *Sci. Transl. Med.* **2**, 57ra83 (2010).
32. L. M. Marquardt, S. C. Heilshorn, Design of injectable materials to improve stem cell transplantation. *Curr. Stem Cell Rep.* **2**, 207–220 (2016).
33. J. R. Beauchamp, J. E. Morgan, C. N. Pagel, T. A. Partridge, Dynamics of myoblast transplantation reveal a discrete minority of precursors with stem cell–like properties as the myogenic source. *J. Cell Biol.* **144**, 1113–1122 (1999).
34. M. Quarta, J. O. Brett, R. DiMarco, A. De Morree, S. C. Boutet, R. Chacon, M. C. Gibbons, V. A. Garcia, J. Su, J. B. Shrager, S. Heilshorn, T. A. Rando, An artificial niche preserves the quiescence of muscle stem cells and enhances their therapeutic efficacy. *Nat. Biotechnol.* **34**, 752–759 (2016).
35. M. Quarta, M. Cromie, R. Chacon, J. Blonigan, V. Garcia, I. Akimenko, M. Hamer, P. Paine, M. Stok, J. B. Shrager, T. A. Rando, Bioengineered constructs combined with exercise enhance stem cell-mediated treatment of volumetric muscle loss. *Nat. Commun.* **8**, 15613 (2017).
36. C. Borselli, C. A. Cezar, D. Shvartsman, H. H. Vandenburgh, D. J. Mooney, The role of multifunctional delivery scaffold in the ability of cultured myoblasts to promote muscle regeneration. *Biomaterials* **32**, 8905–8914 (2011).
37. E. Hill, T. Boontheekul, D. J. Mooney, Designing scaffolds to enhance transplanted myoblast survival and migration. *Tissue Eng.* **12**, 1295–1304 (2006).
38. E. Hill, T. Boontheekul, D. J. Mooney, Regulating activation of transplanted cells controls tissue regeneration. *Proc. Natl. Acad. Sci. U.S.A.* **103**, 2494–2499 (2006).
39. C. A. Rossi, M. Flaibani, B. Blaauw, M. Pozzobon, E. Figallo, C. Reggiani, L. Vitiello, N. Elvassore, P. De Coppi, In vivo tissue engineering of functional skeletal muscle by freshly isolated satellite cells embedded in a photopolymerizable hydrogel. *FASEB J.* **25**, 2296–2304 (2011).
40. J. P. Beier, J. Stern-Straeter, V. T. Foerster, U. Kneser, G. B. Stark, A. D. Bach, Tissue engineering of injectable muscle: Three-dimensional myoblast-fibrin injection in the syngeneic rat animal model. *Plast. Reconstr. Surg.* **118**, 1113–1121 (2006).
41. G. H. Borschel, D. E. Dow, R. G. Dennis, D. L. Brown, Tissue-engineered axially vascularized contractile skeletal muscle. *Plast. Reconstr. Surg.* **117**, 2235–2242 (2006).
42. R. L. Page, C. Malcuit, L. Vilner, I. Vojtic, S. Shaw, E. Hedblom, J. Hu, G. D. Pins, M. W. Rolle, T. Dominko, Restoration of skeletal muscle defects with adult human cells delivered on fibrin microthreads. *Tissue Eng. Part A* **17**, 2629–2640 (2011).
43. C. Fuoco, R. Rizzi, A. Biondo, E. Longa, A. Mascaro, K. Shapira-Schweitzer, O. Kossovar, S. Benedetti, M. L. Salvatori, S. Santoleri, S. Testa, S. Bernardini, R. Bottinelli, C. Bearzi, S. M. Cannata, D. Seliktar, G. Cossu, C. Gargioli, In vivo generation of a mature and functional artificial skeletal muscle. *EMBO Mol. Med.* **7**, 411–422 (2015).
44. C. Fuoco, E. Sangalli, R. Vono, S. Testa, B. Sacchetti, M. V. G. Latronico, S. Bernardini, P. Madeddu, G. Cesareni, D. Seliktar, R. Rizzi, C. Bearzi, S. M. Cannata, G. Spinetti, C. Gargioli, 3D hydrogel environment rejuvenates aged pericytes for skeletal muscle tissue engineering. *Front. Physiol.* **5**, 203 (2014).
45. C. Fuoco, M. L. Salvatori, A. Biondo, K. Shapira-Schweitzer, S. Santoleri, S. Antonini, S. Bernardini, F. S. Tedesco, S. Cannata, D. Seliktar, G. Cossu, C. Gargioli, Injectable polyethylene glycol-fibrinogen hydrogel adjuvant improves survival and differentiation of transplanted mesoangioblasts in acute and chronic skeletal-muscle degeneration. *Skelet. Muscle* **2**, 24 (2012).
46. W. M. Han, Y. C. Jang, A. J. García, Engineered matrices for skeletal muscle satellite cell engraftment and function. *Matrix Biol.* **60–61**, 96–109 (2017).
47. E. A. Phelps, D. M. Headen, W. R. Taylor, P. M. Thulé, A. J. García, Vasculogenic bio-synthetic hydrogel for enhancement of pancreatic islet engraftment and function in type 1 diabetes. *Biomaterials* **34**, 4602–4611 (2013).
48. J. D. Weaver, D. M. Headen, J. Aquart, C. T. Johnson, L. D. Shea, H. Shirwan, A. J. García, Vasculogenic hydrogel enhances islet survival, engraftment, and function in leading extrahepatic sites. *Sci. Adv.* **3**, e1700184 (2017).
49. A. S. Salimath, A. J. García, Biofunctional hydrogels for skeletal muscle constructs. *J. Tissue Eng. Regen. Med.* **10**, 967–976 (2014).
50. E. A. Phelps, N. O. Enemchukwu, V. F. Fiore, J. C. Sy, N. Murthy, T. A. Sulchek, T. H. Barker, A. J. García, Maleimide cross-linked bioactive PEG hydrogel exhibits improved reaction kinetics and cross-linking for cell encapsulation and in situ delivery. *Adv. Mater.* **24**, 64–70 (2012).
51. N. O. Enemchukwu, R. Cruz-Acuña, T. Bongiorno, C. T. Johnson, J. R. García, T. Sulchek, A. J. García, Synthetic matrices reveal contributions of ECM biophysical and biochemical properties to epithelial morphogenesis. *J. Cell Biol.* **212**, 113–124 (2016).
52. L. Lukjanenko, M. J. Jung, N. Hegde, C. Perruisseau-Carrier, E. Migliavacca, M. Rozo, S. Karaz, G. Jacot, M. Schmidt, L. Li, S. Metairon, F. Raymond, U. Lee, F. Sizzano, D. H. Wilson, N. A. Dumont, A. Palini, R. Fässler, P. Steiner, P. Descombes, M. A. Rudnicki, C.-M. Fan, J. von Maltzahn, J. N. Feige, C. F. Bentzinger, Loss of fibronectin from the aged stem cell niche affects the regenerative capacity of skeletal muscle in mice. *Nat. Med.* **22**, 897–905 (2016).
53. A. L. Siegel, K. Atchison, K. E. Fisher, G. E. Davis, D. D. W. Cornelison, 3D timelapse analysis of muscle satellite cell motility. *Stem Cells* **27**, 2527–2538 (2009).
54. H. Liu, A. Niu, S.-E. Chen, Y.-P. Li, β3-integrin mediates satellite cell differentiation in regenerating mouse muscle. *FASEB J.* **25**, 1914–1921 (2011).
55. P. M. Gilbert, K. L. Havenstrite, K. E. G. Magnusson, A. Sacco, N. A. Leonardi, P. Kraft, N. K. Nguyen, S. Thrun, M. P. Lutolf, H. M. Blau, Substrate elasticity regulates skeletal muscle stem cell self-renewal in culture. *Science* **329**, 1078–1081 (2010).
56. P. Lu, K. Takai, V. M. Weaver, Z. Werb, Extracellular matrix degradation and remodeling in development and disease. *Cold Spring Harb. Perspect. Biol.* **3**, a005058 (2011).
57. D. Hardy, A. Besnard, M. Latil, G. Jouvion, D. Briand, C. Thépenier, Q. Pascal, A. Guguin, B. Gayraud-Morel, J.-M. Cavaillon, S. Tajbakhsh, P. Rocheteau, F. Chrétien, Comparative study of injury models for studying muscle regeneration in mice. *PLOS ONE* **11**, e0147198 (2016).
58. G. Le, D. A. Lowe, M. Kyba, Freeze injury of the tibialis anterior muscle. *Methods Mol. Biol.* **1460**, 33–41 (2016).
59. C. F. Bentzinger, Y. X. Wang, J. von Maltzahn, V. D. Soleimani, H. Yin, M. A. Rudnicki, Fibronectin regulates Wnt7a signaling and satellite cell expansion. *Cell Stem Cell* **12**, 75–87 (2013).
60. M. Rozo, L. Li, C.-M. Fan, Targeting β1-integrin signaling enhances regeneration in aged and dystrophic muscle in mice. *Nat. Med.* **22**, 889–896 (2016).
61. E. Ruoslahti, RGD and other recognition sequences for integrins. *Annu. Rev. Cell Dev. Biol.* **12**, 697–715 (1996).
62. J. A. Rowley, D. J. Mooney, Alginate type and RGD density control myoblast phenotype. *J. Biomed. Mater. Res.* **60**, 217–223 (2002).
63. R. Darabi, R. W. Arpke, S. Irion, J. T. Dimos, M. Grskovic, M. Kyba, R. C. R. Perlingeiro, Human ES- and iPS-derived myogenic progenitors restore DYSTROPHIN and improve

Downloaded from http://advances.sciencemag.org/ on July 5, 2019

contractility upon transplantation in dystrophic mice. *Cell Stem Cell* **10**, 610–619 (2012).
64. E. Sleep, B. D. Cosgrove, M. T. McClendon, A. T. Preslar, C. H. Chen, M. H. Sangji, C. M. R. Pérez, R. D. Haynes, T. J. Meade, H. M. Blau, S. I. Stupp, Injectable biomimetic liquid crystalline scaffolds enhance muscle stem cell transplantation. *Proc. Natl. Acad. Sci. U.S.A.* **114**, E7919–E7928 (2017).
65. L. Boldrin, A. Neal, P. S. Zammit, F. Muntoni, J. E. Morgan, Donor satellite cell engraftment is significantly augmented when the host niche is preserved and endogenous satellite cells are incapacitated. *Stem Cells* **30**, 1971–1984 (2012).
66. J. G. Tidball, Regulation of muscle growth and regeneration by the immune system. *Nat. Rev. Immunol.* **17**, 165–178 (2017).
67. A. E. Carpenter, T. R. Jones, M. R. Lamprecht, C. Clarke, I. H. Kang, O. Friman, D. A. Guertin, J. H. Chang, R. A. Lindquist, J. Moffat, P. Golland, D. M. Sabatini, CellProfiler: Image analysis software for identifying and quantifying cell phenotypes. *Genome Biol.* **7**, R100 (2006).
68. M. Rubinstein, R. H. Colby, *Polymer Physics* (Oxford Univ. Press, 2003).

Acknowledgments: We thank the Physiological Research Laboratory and core facilities at the Parker H. Petit Institute for Bioengineering and Bioscience at the Georgia Institute of Technology for the use of shared equipment, services, and expertize. Finally, we thank A. Wagers for providing the *C57Bl/6-β-actin-EGFP* mice. This research was conducted while W.M.H. was a Glenn/American Federation of Aging Research Postdoctoral Fellow. **Funding:** Research reported in this publication was supported by the National Institute of Arthritis and Musculoskeletal and Skin Diseases of the NIH under award numbers R21AR072287 (to Y.C.J.) and R01AR062368 (to A.J.G.). The content is solely the responsibility of the authors and does not necessarily represent the official views of the NIH. This work was also funded by the Parker H. Petit Institute for Bioengineering and Bioscience Seed Grant Program (to A.J.G. and Y.C.J.). **Author contributions:** W.M.H., A.J.G., and Y.C.J. designed the study, analyzed the data, and wrote the manuscript. W.M.H., S.E.A., M.M., D.B., S.A.N., I.F.A., A.P.P., and E.S. conducted the experiments, analyzed the data, and reviewed the manuscript. E.S., S.A.N., and Y.C.J. generated and maintained the animals used in this study. **Competing interests:** The authors declare that they have no competing interests. **Data and materials availability:** All data needed to evaluate the conclusions in the paper are present in the paper and/or the Supplementary Materials. Components for hydrogels may be provided by the Georgia Institute of Technology pending scientific review and a completed material transfer agreement. Requests for these materials should be submitted to A.J.G. Additional data related to this paper may be requested from the authors.

Submitted 3 November 2017
Accepted 11 July 2018
Published 15 August 2018
10.1126/sciadv.aar4008

Citation: W. M. Han, S. E. Anderson, M. Mohiuddin, D. Barros, S. A. Nakhai, E. Shin, I. F. Amaral, A. P. Pêgo, A. J. García, Y. C. Jang, Synthetic matrix enhances transplanted satellite cell engraftment in dystrophic and aged skeletal muscle with comorbid trauma. *Sci. Adv.* **4**, eaar4008 (2018).

Downloaded from http://advances.sciencemag.org/ on July 5, 2019

ScienceAdvances

Synthetic matrix enhances transplanted satellite cell engraftment in dystrophic and aged skeletal muscle with comorbid trauma

Woojin M. Han, Shannon E. Anderson, Mahir Mohiuddin, Daniela Barros, Shadi A. Nakhai, Eunjung Shin, Isabel Freitas Amaral, Ana Paula Pêgo, Andrés J. García and Young C. Jang

Sci Adv **4** (8), eaar4008.
DOI: 10.1126/sciadv.aar4008

ARTICLE TOOLS http://advances.sciencemag.org/content/4/8/eaar4008

SUPPLEMENTARY MATERIALS http://advances.sciencemag.org/content/suppl/2018/08/13/4.8.eaar4008.DC1

REFERENCES This article cites 67 articles, 13 of which you can access for free
http://advances.sciencemag.org/content/4/8/eaar4008#BIBL

PERMISSIONS http://www.sciencemag.org/help/reprints-and-permissions

Use of this article is subject to the Terms of Service

Science Advances (ISSN 2375-2548) is published by the American Association for the Advancement of Science, 1200 New York Avenue NW, Washington, DC 20005. 2017 © The Authors, some rights reserved; exclusive licensee American Association for the Advancement of Science. No claim to original U.S. Government Works. The title *Science Advances* is a registered trademark of AAAS.

Downloaded from http://advances.sciencemag.org/ on July 5, 2019